

Grain textural bias in detrital single-mineral provenance studies

Xiaotian Shen^a, Xing Jian^{a,*}, Wei Zhang^a, Ping Guan^b

^a State Key Laboratory of Marine Environmental Science, College of Ocean and Earth Sciences, Xiamen University, Xiamen 361102, PR China

^b MOE Key Laboratory of Orogenic Belts and Crustal Evolution, School of Earth and Space Sciences, Peking University, Beijing 100871, PR China

ARTICLE INFO

Article history:

Received 30 May 2024

Received in revised form 9 August 2024

Accepted 11 August 2024

Available online 16 August 2024

Editor: Dr. Basilici Giorgio

Keywords:

Detrital zircon geochronology

Detrital single-mineral geochemistry

Sedimentary provenance analysis

Grain textural bias

Hydraulic sorting

ABSTRACT

Detrital single-mineral geochemistry and geochronology are strong tools in provenance studies and indicate great potentials in addressing issues in earth sciences. Various biases (both natural and artificial) exist objectively and may mislead provenance interpretations. Both the sedimentary sorting process and hand-picking in-laboratory processing may lead to analyzed grain textural (e.g., size and shape) variability and thus may introduce biases in single-mineral provenance analysis. Here, we take the Mesozoic–Cenozoic Qaidam basin, northeastern Tibet, as an example to investigate the relationship between single-mineral grain texture and detrital zircon geochronological and detrital tourmaline, rutile and garnet geochemical data and to explain how grain texture affects detrital single-mineral provenance interpretations. Results indicate that Precambrian zircons take less proportions in coarse ($>125\ \mu\text{m}$), subrounded and high aspect ratio (>2) fractions than Phanerozoic zircons. Parent rock lithology discrimination results of detrital tourmaline and garnet in different grain size fractions show significant differences. Zr-temperature values of detrital rutile have an increasing trend with increasing grain size. The geochemistry of detrital tourmaline, rutile and garnet shows no dependence with grain aspect ratio and roundness. We suggest that inheritance of grain texture features from parent rocks is the major reason. Detrital zircons from recycled (meta)sedimentary rocks tend to be smaller and more rounded than those from igneous rocks. Detrital tourmaline, rutile and garnet grains from different parent rock types vary in size. Grain textural bias may cause the underestimated contributions of the Qilian Shan to the Cenozoic Qaidam basin if small detrital zircons were not involved in the analysis. Quantitative description of the source-to-sink system of the Cenozoic Qaidam is also influenced by grain textural bias. This study highlights the underestimated grain textural bias in single-mineral provenance studies. We suggest that a comprehensive understanding of potential sedimentary sources, depositional processes, sample petrographic features and laboratory analysis procedures is important to reliable provenance interpretations and to related implications in earth sciences.

© 2024 Elsevier B.V. All rights are reserved, including those for text and data mining, AI training, and similar technologies.

1. Introduction

Sedimentary provenance is a crucial topic in earth science studies and has extensive applications in a variety of fields, including but not limited to plate tectonics, paleoclimatology, sedimentary geology, petroleum geology and early Earth evolution studies (Dickinson, 1985; Cawood et al., 2003; Weltje and von Eynatten, 2004; Nie et al., 2012; Caracciolo, 2020). Provenance does not only refer to sediment source terranes and parent rock lithologies but also involves various complex physiochemical modifications during sediment generation, dispersal, deposition and diagenesis processes (Johnsson, 1993; Weltje and von Eynatten, 2004; Weltje, 2012). Weathering, topography, climatic condition, tectonic activity, transport agent type, hydraulic sorting, recycling,

abrasion, compaction, diagenetic fluid and many other factors may contribute to the formation of detrital products and thus leave fingerprints in sediments and sedimentary rocks (Morton et al., 2005; Garzanti et al., 2008, 2009, 2018; Caracciolo, 2020).

Since the late 19th century, a growing number of tools have been applied in analyzing sediment and sedimentary rock and in unraveling sedimentary provenance (Sorby, 1880; Henry and Guidotti, 1985; Pettijohn et al., 1987; Weltje and von Eynatten, 2004, and references therein). Traditional methods, such as sandstone framework composition, accessory mineral assemblages, clay mineralogy, bulk geochemistry and isotopic geochemistry, were widely used for reconstructing detrital parent rock lithologies and tectonic settings of the source area (Chayes, 1949; Griffiths, 1967; McBride, 1963; Folk, 1968; Dickinson, 1970, 1985; Dickinson and Suczek, 1979; Bhatia, 1983; Bhatia and Crook, 1986; McLennan et al., 1993; Taylor and McLennan, 1995). However, these approaches based on bulk samples or specific grain-size window analysis have limitations in some cases, like 1) when sediments

* Corresponding author.

E-mail address: xjian@xmu.edu.cn (X. Jian).

represent mixing products of multiple sources (Jian et al., 2013b; Garzanti et al., 2014), precisely discriminating contributions from different sources via these approaches is difficult; 2) hydraulic sorting may filter relevant signals from parent rocks and affect mineral and elemental compositions of sediments (Garzanti et al., 2008, 2009; von Eynatten et al., 2012); and 3) intensive weathering or diagenesis processes alter sediment compositions (Nie et al., 2012; Garzanti et al., 2018).

In contrast to bulk analysis, elemental or isotopic composition of single grains of a single-mineral phase is assumed to be rarely fractionated due to mechanical and chemical processes, especially for stable detrital minerals. Individual mineral-phase variability is helpful to identify contributions from multiple sources (von Eynatten and Dunkl, 2012). In recent decades, in-situ single mineral-based provenance analysis got fast developed with availability of sophisticated techniques, such as the sensitive high-resolution ion microprobe (SHRIMP), laser ablation inductively-coupled plasma mass spectrometry (LA-ICP-MS) and secondary ion mass spectrometry (SIMS; Mange and Morton, 2007; Meinhold et al., 2008; von Eynatten and Dunkl, 2012). Based on those, in-situ analysis not only obtains high-resolution elemental and isotopic compositions of any detrital minerals, but also provides benefits for avoiding weathered or diagenetically altered detrital grains. Both accessory minerals (e.g., zircon, tourmaline, rutile, garnet, spinel, apatite, amphibole) and framework grains (e.g., quartz, feldspar) from siliciclastic sediments can be targeted for single-grain provenance analysis (Morton, 1985, 1991; Clift et al., 2001; von Eynatten and Dunkl, 2012; Blowick et al., 2019). Compared with weathering-sensitive feldspar and chemically-invariable quartz, some stable accessory minerals, such as zircon, tourmaline, rutile and garnet, have diverse chemical compositions and demonstrate great potentials in tracing sediment provenance (von Eynatten and Dunkl, 2012; Hu et al., 2016; Deng et al., 2017; Zoleikhaei et al., 2021). Various geochemical and/or geochronological indexes of these four minerals have been widely used in provenance studies (Table 1; see details in Appendix B), such as zircon U–Pb geochronology for source terrane tectono-magmatic history (Gehrels, 2014), and tourmaline, rutile and garnet element geochemistry for parent rock lithology discrimination (Henry and Guidotti, 1985; Mange and Morton, 2007; Triebold et al., 2012). Furthermore, some new provenance-indicators of these four minerals have been proposed and developed in recent years providing deep understanding in single-mineral provenance analysis (Table 1; Tolosana-Delgado et al., 2018; Guo et al., 2021; Schönig et al., 2021; Hu et al., 2023; Triantafyllou et al., 2023).

Many natural processes potentially introduce biases in single-mineral provenance analysis (Malusà et al., 2013; Chew et al., 2020; Guo et al., 2020; Caracciolo et al., 2021). Hydraulic sorting is a common source of bias because of differential settling of clastic grains depending on their grain size, shape and density (Rubey, 1933; Garzanti et al.,

2009; Deal et al., 2023). According to the settling-equivalence principle, coarse and low-density grains tend to be deposited with fine dense grains. This causes composition variability in sediments under different energy conditions with identical sources (Garzanti et al., 2008). Mineral fertility variation is also considered as a major source of bias (Malusà et al., 2016; Chew et al., 2020). Using zircon as an example, the amounts of zircon grains yielding from different parent rocks could differ by orders of magnitude (Dickinson, 2008; Malusà et al., 2016). Similarly, erosion-rate variation among catchments, which are affected by lithologies (sedimentary rocks vs igneous rocks vs metamorphic rocks), tectonic activity (active vs inactive), climate (arid vs humid) and geomorphology (steep vs flat), is also a source of bias (Harel et al., 2016; Malusà et al., 2009; Resentini et al., 2017; Caracciolo, 2020). Diagenesis bias is also common in deep-time sedimentary provenance analysis because mineral suites can change due to different compositions of fluid and selected dilution of relatively unstable minerals under increasing pressure–temperature conditions (Morton and Hallsworth, 2007; Garzanti et al., 2018). In addition, intrinsic properties of mineral grains could lead to specific selection. For example, zircon grains with high U contents can cause radiation damage which leads a grain to become metamict and thus fragile in weathering processes (Malusà et al., 2013). Analytical biases during sampling, laboratory procedures and data handling are commonly realized, but often subjectively ignored and little quantitatively described (Andersen, 2002; Sircombe and Stern, 2002; Vermeesch, 2004, 2012; Andersen et al., 2019).

Grain texture (such as grain size, roundness and aspect ratio) has been found to potentially introduce bias in single-mineral provenance analysis in many ways (Yang et al., 2012; Chew et al., 2020; Leary et al., 2020; Castillo et al., 2022; Zutterkirch et al., 2022; Feil et al., 2024). Firstly, the grain texture effect is commonly noticed due to the vital role in hydraulic sorting (Lawrence et al., 2011; Malusà et al., 2013; Muhlbauer et al., 2017). If mineral geochronology or geochemistry is related to grain texture, sediments from a specific source with different grain texture may vary largely in chemical composition or age populations (e.g., Lawrence et al., 2011). Secondly, grain texture inherited from different parent rocks may be distinct (Krippner et al., 2015; Liang et al., 2023; Feil et al., 2024). Handpicking or handling of sample during in-laboratory processes may be preferential for specific grain texture (Chew et al., 2020; Dröllner et al., 2021; Zutterkirch et al., 2022). Many studies have noticed the influence of grain size and have tested whether grain size influences the single-mineral provenance analysis results by comparing features of grains within different sizes (e.g., Viator, 2003; von Eynatten et al., 2005; Yang et al., 2012; Malusà et al., 2013; Krippner et al., 2016; Cantine et al., 2021). However, the relationship between grain size and single-mineral provenance interpretation remains controversial. In some cases, detrital zircon U–Pb

Table 1

Basic description of zircon, tourmaline, rutile and garnet and related provenance indicators.

	Zircon	Tourmaline	Rutile	Garnet
General formula	Zr[SiO ₄]	XY ₃ Z ₆ (BO ₃)Si ₆ O ₁₈ (OH) ₄ ^a	TiO ₂	X ₃ Y ₂ (SiO ₄) ₃ ^b
Crystal system	Tetragonal system	Trigonal system	Tetragonal system	Cubic system
Potential sources	Intermediate–medium igneous rocks Medium–high grade metamorphic rocks Recycled sedimentary rocks	Granitoids Pegmatites Aplites Metasedimentary rocks Hydrothermal deposits	Granites Pegmatites Medium–high grade metamorphic rocks Recycled sedimentary rocks	Low–high grade metamorphic rocks Igneous rocks Ultramafic rocks
Provenance indicators	U–Th–Pb geochronology Hf and O isotope Ti-in-zircon thermometer Eu anomalies Fission-track thermochronology (U–Th)/He thermochronology REE and trace elements	Major elements B isotope	Trace elements Zr-temperature U–Pb geochronology	Major elements Trace elements Sm–Nd geochronology

^a X for Na, Ca, K or vacancy; Y for Mg, Fe, Mn, Al, or Li; Z for Al, Mg, Fe, Cr or V.

^b X for Mg, Fe²⁺, Mn, or Ca; Y for Al, Cr, Ti, or Fe³⁺.

age distributions as well as garnet geochemical data were found to be related to grain size (e.g., Viator, 2003; Lawrence et al., 2011; Yang et al., 2012; Krippner et al., 2015), while some cases concluded a different opinion (e.g., von Eynatten et al., 2005; Malusà et al., 2013; Muhlbauer et al., 2017). Compared to grain size, the influence of aspect ratio and roundness is scarcely discussed (Malusà et al., 2013; Muhlbauer et al., 2017; Leary et al., 2020; Castillo et al., 2022), which may be due to the lack of commonly-used quantitative methods. Based on the investigation of detrital zircon U–Pb ages from the modern European rivers, it is found that zircon grains with young ages are comparatively abundant in the high aspect ratio fraction (Malusà et al., 2013; Castillo et al., 2022). Overall, the role of grain texture in single-mineral provenance analysis still needs further discussion.

The Qaidam basin, located in the northern Tibetan plateau, represents a large intermountain basin bounded by the Qilian Shan, East Kunlun Shan and Altyn Shan (Fig. 1) and holds thick sedimentary records supplied by adjacent mountains. Because the northern and eastern parts of the Qaidam basin are mainly fed by the Qilian Shan (Jian et al., 2013a) which contains diverse igneous and metamorphic rocks (contributing abundant zircon, tourmaline, rutile and garnet grains (Jian et al., 2013a)), this region can be an ideal area to investigate potential grain textural bias in detrital single-mineral provenance interpretation. In this study, we take the northern and eastern Mesozoic–Cenozoic Qaidam basin as an example, targeting detrital zircon, tourmaline, rutile and garnet, to integrate published geochronological and geochemical data and to quantify detrital grain textural parameters (grain size, aspect ratio, roundness). The aims are to 1) explore the relationship between detrital grain textural features and geochronological and geochemical data and 2) try to explain how grain texture affects detrital single-mineral provenance interpretations.

2. Geological setting

The Qaidam basin contains 3–16 km thick Mesozoic and Cenozoic sedimentary successions and covers approximately 120,000 km² (Zhuang et al., 2011; Jian et al., 2013b, 2020). The Mesozoic sedimentary successions of the Qaidam basin are commonly divided into six

stratigraphic units, as shown in Fig. 2. Mesozoic strata in the eastern and northern Qaidam basin are regarded to accumulate in fluvial and alluvial environments (Wu et al., 2011), characterized by sandstone–mudstone suits and red conglomerates. The Cenozoic strata in the northern Qaidam basin are commonly divided into seven units (Fig. 2) and were mainly deposited in fluvial and lacustrine depositional environments. These strata mainly contain fine-coarse sandstones with some conglomerates and generally display coarse (Lulehe formation)–fine (Xia Ganchaigou–Shang Youshashan formation)–coarse (Shizigou and Qigequan formation) grained changes in ascending order (Jian et al., 2023), revealing temporal variations in sedimentary environments.

The Qilian, Altyn, and East Kunlun Mountains surround the Qaidam basin (Fig. 1) and are considered the source areas for the Qaidam basin. The Qilian Shan is mainly composed of the Precambrian to Lower Paleozoic metamorphic rocks, early Paleozoic granitic rocks, marine sedimentary strata as well as a small amount of ophiolitic suites (Fig. 1A; Gehrels et al., 2003; Jian et al., 2013a; Song et al., 2013, 2014; Zhang et al., 2020). The East Kunlun Shan mainly consists of the Early Cambrian to Early Devonian and Late Permian–Triassic granitoid plutons and Devonian to Early Triassic marine sedimentary rocks (Dai et al., 2013; Huang et al., 2014; Jian et al., 2018). The Altyn Shan mainly hosts Ordovician metasedimentary rocks, Jurassic sedimentary rocks, and Paleozoic and Mesozoic granite rocks (Yang et al., 2006; Mattinson et al., 2010; Jian et al., 2013a).

Provenance of the Mesozoic and Cenozoic deposits in the Qaidam basin has been discussed in numerous studies via various methods (e.g., Ritts and Biffi, 2001; Rieser et al., 2005; Jian et al., 2013a, 2013b; Bush et al., 2016; Cheng et al., 2016; Bao et al., 2019; Yan et al., 2024). Based on the paleocurrent orientation, petrographic analysis, single-mineral geochronology and geochemistry, the sandstones in the northern and eastern Qaidam basin are proposed to be mainly contributed by the nearby Qilian Shan (Rieser et al., 2005; Jian et al., 2013a, 2013b, 2024; McRivette et al., 2019; Sun et al., 2020; He et al., 2021). Jian et al. (2013a) further divided the northern and eastern Qaidam into three depositional areas with different contributions from various grades of metasedimentary rocks and intermediate-acidic igneous rocks within the Qilian Shan. The temporal variations of provenance of

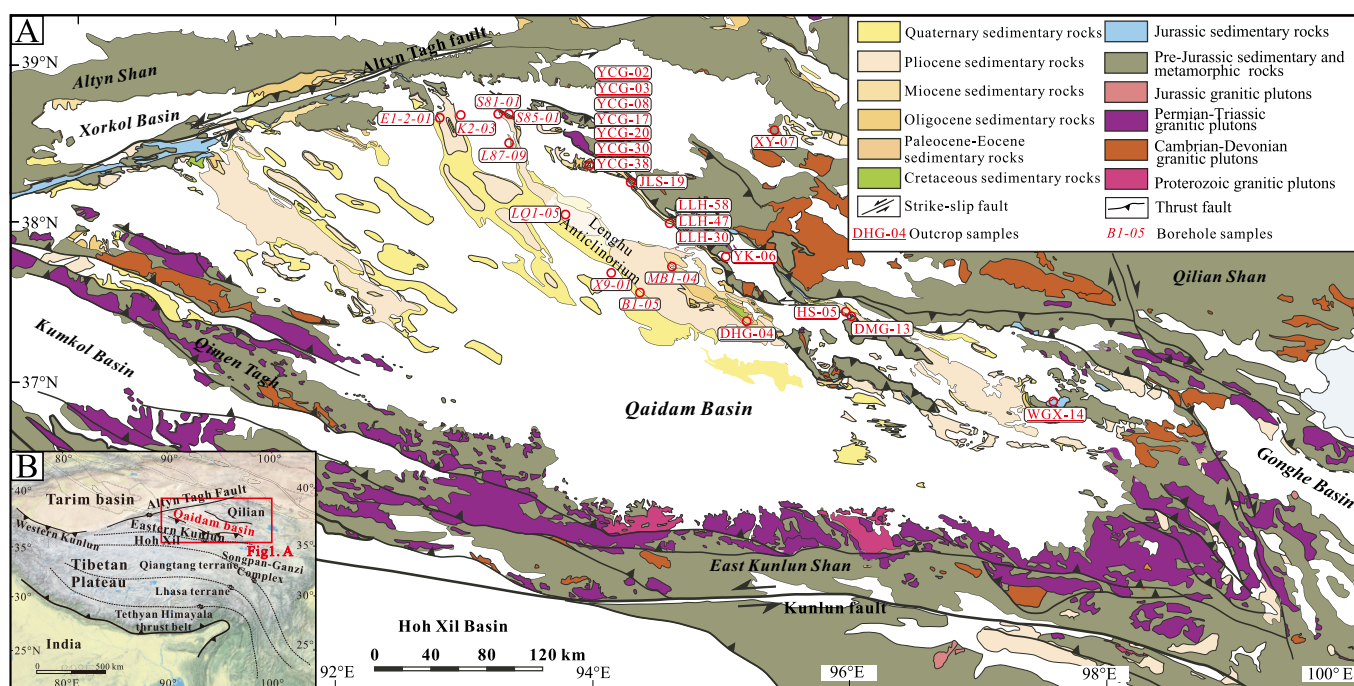


Fig. 1. Geological map (A) and locations (B) of the Qaidam basin (modified from Lu et al., 2019). Abbreviations: YCG: Yingchaogou section; JLS: Jielsu section; LLH: Lulehe section; XY: Xiangyang section; YK: Yuka section; DHG: Dahonggou section; HS: Hongshan section; DMG: Dameigou section; WGX: Wanggaxiu section.

Era	Period	Epoch	Formation	Sample				Depositional Environment & lithologic description	
				Zircon	Tourmaline	Garnet	Rutile		
Cenozoic	Quaternary	Holocene		n=12	n=7	n=17	n=7	Alluvial fan and salt lake environments. Conglomerates, sandstones and evaporites.	
		Pleistocene	Qigequan Fm.						
	Neogene	Pliocene	Shizigou Fm.			LLH-58	LLH-58	Alluvial fan and occasionally fluvio-lacustrine environments. Conglomerates, sandstones and occasionally mudstones and evaporites.	
		Miocene	Shang Youshashan Fm.	B1-05 YCG-38			B1-05 YCG-38		
			Xia Youshashan Fm.	YCG-30 LQ1-05	LLH-47		YCG-30 LQ1-05 LLH-47		
	Paleogene	Oligocene	Shang Ganchaigou Fm.	L87-09 YCG-20	YCG-17 X9-01		YCG-17 L87-09 K2-03 X9-01	Fluvial, deltaic and lacustrine environments. Fine-grained sandstones and mudstones with subordinate carbonate and evaporite layers.	
		Eocene	Xia Ganchaigou Fm.	YCG-03 L87-02	YCG-08 B1-01		YCG-08 YCG-02 MB1-04 JLS-19		
		Paleocene	Lulehe Fm.	DHG-04 EI-2-01 LLH-30 HS-05		LLH-30	S81-01 LLH-30	Alluvial fan and plain environments. Red conglomerates with carbonate and evaporite layers.	
	Mesozoic	Cretaceous	Late	Lack of sediments and erosion phase?					
			Early	Quanyagou Fm.				LLH-20	Alluvial fan and fluvial environments. Red conglomerates, sandstones and occasionally mudstone layers.
Jurassic		Late	Hongshuigou Fm.				WGX-14	Fluvial, deltaic and occasionally marginal lacustrine environments. Red sandstone-mudstone suits.	
		Middle	Caishiling Fm. Dameigou Fm.				YK-06 XY-07 JLS-07 LI-05	Fluvial, deltaic, swamp and lacustrine environments. Sandstones, mudstones and coal beds.	
		Early	Xiaomeigou Fm. Huxishan Fm.				S85-01 DMG-13		

Fig. 2. Mesozoic and Cenozoic stratigraphy framework, depositional environment and lithological description of the Qaidam basin. (Modified from Jian et al. (2013b).)

the Cenozoic Qaidam basin are caused by the variable contributions from different micro-terraces in the Qilian Shan, which is not only related to tectonic evolution of the source area, but also to lithology heterogeneity of source terranes, recycling, hydrodynamic sorting and sedimentary environment (Jian et al., 2024).

3. Samples and methods

Thirty-one Mesozoic–Cenozoic sandstone samples from 7 boreholes and 8 outcrops in the northern Qaidam basin were selected for detrital single-mineral provenance analysis and grain texture measurement (Figs. 1–2). Twelve Cenozoic samples were used for detrital zircon U–Pb geochronology analysis, and U–Pb ages and grain size and aspect ratio data were published (Jian et al., 2023, 2024). Seven Cenozoic samples were used for detrital tourmaline geochemistry analysis (Fig. 2; samples X9-01, B1-01, YCG-08 and YCG-17 were reported in Jian et al., 2013a). Detrital rutile grains were from seven Mesozoic samples to obtain trace-element composition (new data in this study). Detrital garnet grains were selected from sixteen Cenozoic and one Mesozoic samples for obtaining major-element composition (reported in Jian et al., 2013a except sample S85-01). Roundness of analyzed zircon grains and grain textural data of detrital tourmaline, rutile and garnet were not published. Partial samples were previously analyzed for petrographic and heavy mineral assemblages (Jian et al., 2013a; Table S1 in Appendix A). All samples are fine- to coarse-grained sandstone and are poorly–moderately sorted, with mainly angular to subangular grains, dominated by quartz and (meta)sedimentary lithic fragments (Jian et al., 2013a, 2013b, 2023; Table S1). Garnet dominates the transparent heavy-mineral fraction in most samples (7.6–48.5%; Table S1); zircon, tourmaline and rutile are subordinate components (<10%; Jian et al., 2013a).

All detrital grains were first randomly handpicked from sandstone samples under a microscope, then fixed on the target by epoxy resins, grounded, and polished for subsequent analysis. The heavy mineral separation was described by Jian et al. (2013a). All grains were first pictured under a polarizing microscope for grain textural feature measurements. Grains with apparent fresh fracture which may be caused by anthropogenic breaking were excluded. Detrital zircon U–Pb geochronological analyses were performed at Nanjing Normal University (samples LLH-30, DHG-04 and HS-05; using an Agilent 7500a ICP-MS equipped with a New Wave 213-nm laser) and Peking University (remaining 9 samples; using an Agilent 7500a ICP-MS coupled with a 193-nm laser). The ablation pit depth was 20–40 μm with a 32 μm diameter beam carried by helium gas. Plešovice (337 Ma) and 91500 (1062 Ma) were simultaneously measured as standard reference materials for U–Th–Pb geochronology and other trace elements. Isotopic ratios were subsequently calculated by the GLITTER software and common-Pb was corrected by the method proposed by Andersen (2002). After initial-Pb correction, $^{207}\text{Pb}/^{206}\text{Pb}$ ratios were adopted for grains older than 1000 Ma, whereas $^{206}\text{Pb}/^{238}\text{U}$ ratios were adopted for grains younger than 1000 Ma. Data with precision > ±10% and discordance > ±10% were omitted in further discussion. The major elemental geochemistry of detrital garnet and tourmaline was obtained at Peking University using a JEOL JXA 8100 Electron Probe Microanalyzer. Analytical conditions were at 15 kV accelerating voltage with a 10 nA focused beam current and 1 μm diameter beam for all the elements (detailed operation and calibration refer to Song et al., 2007; Zhang et al., 2008). The trace-elemental data of detrital rutile were obtained by using a LA-ICP-MS at Peking University. The analytical conditions are 44 μm diameter beam, 20–40 μm ablation pit depth and helium gas carrier. NIST SRM 610 was employed as the standard for instrument calibration.

The grain sizes of grains were represented by the equivalent spherical diameter (nominal diameter, Garzanti et al., 2008), based on transmitted-light photomicrographs of the grains after mounting and polishing. The longest axis of a grain is regarded as the length (X) and its perpendicular and bisected axis is the width (Y), and the third axis (Z) is assumed to be the same as the width. The grain size of each grain equals $(X \cdot Y \cdot Z)^{1/3}$ (Lawrence et al., 2011). The aspect ratio (defined as length/width ratio) calculation is to quantify the shape of each grain. Roundness of a mineral grain is defined as the average radius of curvature of all corners of the grain in one section divided by the radius of the largest inscribed circle in that section (Wadell, 1932). The Matlab script of Resentini et al. (2018) was used for automatically obtaining grain roundness values that correspond to six roundness grades: very angular (0.12–0.17), angular (0.17–0.25), subangular (0.25–0.35), subrounded (0.35–0.49), rounded (0.49–0.7), and well rounded (0.7–1.0).

Detrital zircon U–Pb geochronological data were processed by the DensityPlotter program (Vermeesch, 2012) and IsoplotR program (Vermeesch, 2018) to obtain U–Pb age Kernel Density Estimation plots and cumulative age distributions (CAD). The provenance interpretations of detrital tourmaline geochemical data were followed by the Al–Fe(tot)–Mg ternary discrimination diagram (Henry and Guidotti, 1985). Several distinct regions can be defined for tourmaline from different rocks, including Li-poor granite, Li-rich granite, Fe-rich granite, metasedimentary rocks (metapelite or metapsammite), Fe-rich rocks, metacarbonates and low-Ca ultramafic rocks. Parent rock lithology discriminations of detrital rutile were based on the Cr–Nb diagram (Meinhold et al., 2008), which classifies rutile from metamafic and metapelitic rock. The calculation of Zr-in-rutile followed the formula in the α -quartz field from Tomkins et al. (2007). Garnet geochemical data were recalculated to six end-members (pyrope, almandine, spessartine, grossular, andradite, uvarovite). Two parent rock lithology discrimination methods were used for detrital garnet major-element composition. One is the Mg–Fe²⁺ + Mn–Ca (i.e., pyrope-almandine + spessartine-grossular + andradite) ternary diagram proposed by Mange and Morton (2007). This diagram is divided into five fields for garnet from different rocks, including granulite-facies and amphibolite-facies metasedimentary rocks, intermediate-acidic igneous rocks, meta-basic rocks, and metasomatic rocks. The other is a hierarchical scheme based on the major element composition of garnet which gives the probabilities of the parent rock (including five types: eclogite-facies, amphibolite-facies and granulite-facies metamorphic rocks, ultramafic rocks and igneous rocks; Tolosana-Delgado et al., 2018).

The Kolmogorov–Smirnov (K–S) test was used to evaluate the dissimilarity of detrital zircon U–Pb age distributions of different fractions following the formula of Vermeesch (2013) and Malusà et al. (2013). The significance level α was 0.05. The test results were described by the V_{K-S} value, i.e., if $V_{K-S} > 0$, differences between two distributions are not statistically significant; otherwise, two curves are statistically different. Pearson's chi-squared test, a statistical hypothesis test used to examine whether two categorical variables are independent, was applied for identifying whether the parent rock lithology distribution differences of detrital tourmaline, rutile and garnet are dependent on grain texture. Fractions that have the number of grains smaller than 40 were not involved in the statistical test. The null hypothesis, i.e., two variables (parent rock lithology and grain texture) are independent, was accepted when the p-value is >0.05 .

4. Results

4.1. Detrital zircon

A total of 1000 detrital zircon U–Pb ages were obtained. The U–Pb ages include two dominating Phanerozoic age groups, i.e., 350–500 Ma (40%) and 200–350 Ma (20%), and three subordinate Precambrian age groups, i.e., 700–1100 Ma (18%), 1500–2150 Ma (13%) and 2300–2950 Ma (9%) (Fig. S1A in Appendix B). The grain size and aspect

ratio of all the dating grains were measured, and roundness quantitative data of 317 grains from four samples (L87-09, LQ1-05, YCG-20, E1-2-01) were obtained. The analyzed detrital zircon grains cover a size range from 32 to 239 μm , with 79% very fine sand grains (63–125 μm ; Figs. 3–4). Zircons larger than 125 μm only take about 13% of all zircon grains and another 18% are within 32–63 μm (Fig. 4A). Analyzed grains were divided into three fractions based on aspect ratio data, including aspect ratios of 1–1.5 (51%), 1.5–2 (34%) and >2 (15%; Fig. 4C). Rounded zircon grains are dominant and make up 62% of all grains, with the subordinate subrounded fraction (31%) and minor well rounded fraction (7%; Fig. 4B).

Detrital zircon grains from the three grain size fractions show significant variation of U–Pb age distributions with a negative V_{K-S} value between 125–250 μm and other two fractions (Figs. 5–6). The proportion of Precambrian zircon grains (>540 Ma) decreases from 45% in the 32–63 μm fraction to 39% in 63–125 μm and 25% in 125–250 μm fractions (Fig. 5A–B). Significant differences are found among zircon U–Pb age distributions of three aspect ratio fractions (all three V_{K-S} values < 0 ; Figs. 5C, 6B). The proportions of young 200–350 Ma zircon grains increase with increasing aspect ratio, while old 1500–2150 Ma and 2300–2950 Ma groups decrease (Fig. 5C–D). The difference between age distributions of two major roundness fractions is not significant ($V_{K-S} > 0$; Fig. 6B), but the proportion of 200–350 Ma is decreasing from subrounded (31%) to rounded (25%) and well rounded (18%; Fig. 5E).

4.2. Detrital tourmaline

A total of 263 detrital tourmaline geochemical data from seven samples were analyzed. In the Al–Fe–Mg ternary diagram, about 72% of all the analyzed tourmalines have Al/(Al + Fe + Mg) values above 33% and Mg/(Al + Fe + Mg) values above 26% which are from metasedimentary (metapelites or metapsammites) rocks (Fig. 7; Table S3). Tourmaline grains with Mg/(Al + Fe + Mg) values below 26% (classified as granite-sourced tourmaline) are subordinate components (25%) and Fe-rich rock-sourced tourmaline grains only take 3% (Fig. 7). The grain size and aspect ratio of all analyzed tourmaline grains were measured, and roundness of 154 grains from four samples (B1-01, X9-01, YCG-08, YCG-17) was obtained. Based on grain size, analyzed tourmaline grains were separated into two fractions, including the dominating 63–250 μm fraction (75%) and subordinate 250–500 μm (25%) fraction (Fig. 4D). About 73% tourmaline grains have aspect ratios below 1.5, 22% above 1.5 and below 2, and only 5% grains have aspect ratios higher than 2 (Fig. 4F). Subrounded (43%) and rounded (39%) fractions dominated in analyzed grains (Fig. 4E). Subangular and well rounded fractions only make up for 7% and 9%.

Tourmaline in the 63–250 μm fraction is composed of dominating metamorphic rock-sourced tourmaline grains (77%) and granite-sourced grains (21%) with a few Fe-rich rock-sourced grains (2%; Fig. 7A). Constituents of the 250–500 μm fraction are made up of 56% metamorphic rock-sourced and 38% granite-sourced and 6% Fe-rich-sourced grains (Fig. 7A). Pearson's chi squared test result indicates close relationships between grain size and detrital tourmaline sources (p-value = 0.0000319 < 0.05 ; Table 2). Two major aspect ratio fractions are also similar in tourmaline components (Fig. 7B) with a p-value (0.7633) above 0.05 (Table 2). Tourmaline components in four roundness fractions are similar (Fig. 7C). The subrounded fraction consists of 62% metamorphic rock-sourced, 36% granite-sourced and 2% Fe-rich-sourced grains, and the rounded fraction is 33%, 60% and 7%, respectively (Fig. 7C). The difference between subrounded and rounded groups is not significant as indicated by Pearson's chi squared test (p-value = 0.3316 > 0.05 ; Table 2).

4.3. Detrital rutile

Trace element composition of 248 rutile grains was obtained. Grains with Nb content above 800 ppm and higher than Cr content were the



Fig. 3. Representative photomicrographs of detrital zircon, tourmaline, rutile and garnet with diverse grain texture and chemical compositions as well as parent rock lithology or U–Pb ages.

major components (57%) which were typical for rutile from metapelitic rocks (Fig. 8). The other 43% grains having Nb content below 800 ppm or lower than Cr content are from metamafic rocks. The Zr-temperature of all grains covers a range from 468.3 to 930.4 °C, with the average of 649.5 °C (Fig. 9). The grain size and aspect ratio of all analyzed rutile grains were measured, and 109 grains from five samples (WGX-14, DMG-13, XY-07, YK-06, L1-05) were chosen to quantify roundness. Most grains are from 63 to 250 μm (77% 63–125 μm and 20% 125–250 μm; Fig. 4G). According to aspect ratio, rutile grains were separated into three fractions, including 1–1.5 (58%), 1.5–2 (31%) and >2 (11%; Fig. 4I). The analyzed grains were mainly characterized by rounded (52%) and subrounded (34%), with minor well rounded grains (8%; Fig. 4H).

Rutile components in two major size fractions are close and not significantly different (p -value = 0.373 > 0.05). The 63–125 μm fraction consists of 44% metamafic and 56% metapelitic rutile, and the 125–250 μm fraction contains 40% metamafic and 60% metapelitic rutile (Fig. 8A). There is a slight difference between the aspect ratio 1–1.5 fraction and other two fractions, while aspect ratio 1.5–2 and >2 fractions are almost the same (Fig. 8B). Metamafic rutile takes up higher proportions in the aspect ratio 1–1.5 fraction (47%) than aspect ratio 1.5–2 (37%) and >2 (36%) fractions. Subrounded and rounded fractions

are similar, which have 51% and 54% metapelitic rutile, respectively (Fig. 8C). Zr-temperature values of detrital rutile show a certain relationship with grain size (Fig. 9A), indicating that rutile grains with large grain size are featured by high average and maximum Zr-temperature. There is no correlation between roundness and aspect ratio and Zr-temperature of detrital rutile.

4.4. Detrital garnet

All the analyzed 666 garnet grains are diverse in chemical compositions. The calculation of six end-members revealed that almandine (26–91 mol%, average 67 mol%) is dominating, and pyrope (1–43 mol%, average 14 mol%), grossular (0–44 mol%, average 10 mol%) and spessartine (0–58%, average 8 mol%) are subordinates, with minor andradite (0–9 mol%) and uvarovite (0–2 mol%). Overall, the analyzed garnet grains are dominantly falling in intermediate-acidic igneous rocks or amphibolite-facies rocks (79%) in the Mg–Fe²⁺ + Mn–Ca diagram (Mange and Morton, 2007; Fig. 10A). These Fe + Mn-rich, Mg-poor and Ca-poor grains are thought to be from amphibolite-facies rocks rather than intermediate-acidic igneous rocks according to previous trace element discrimination results (Hong et al., 2020). Garnet grains from

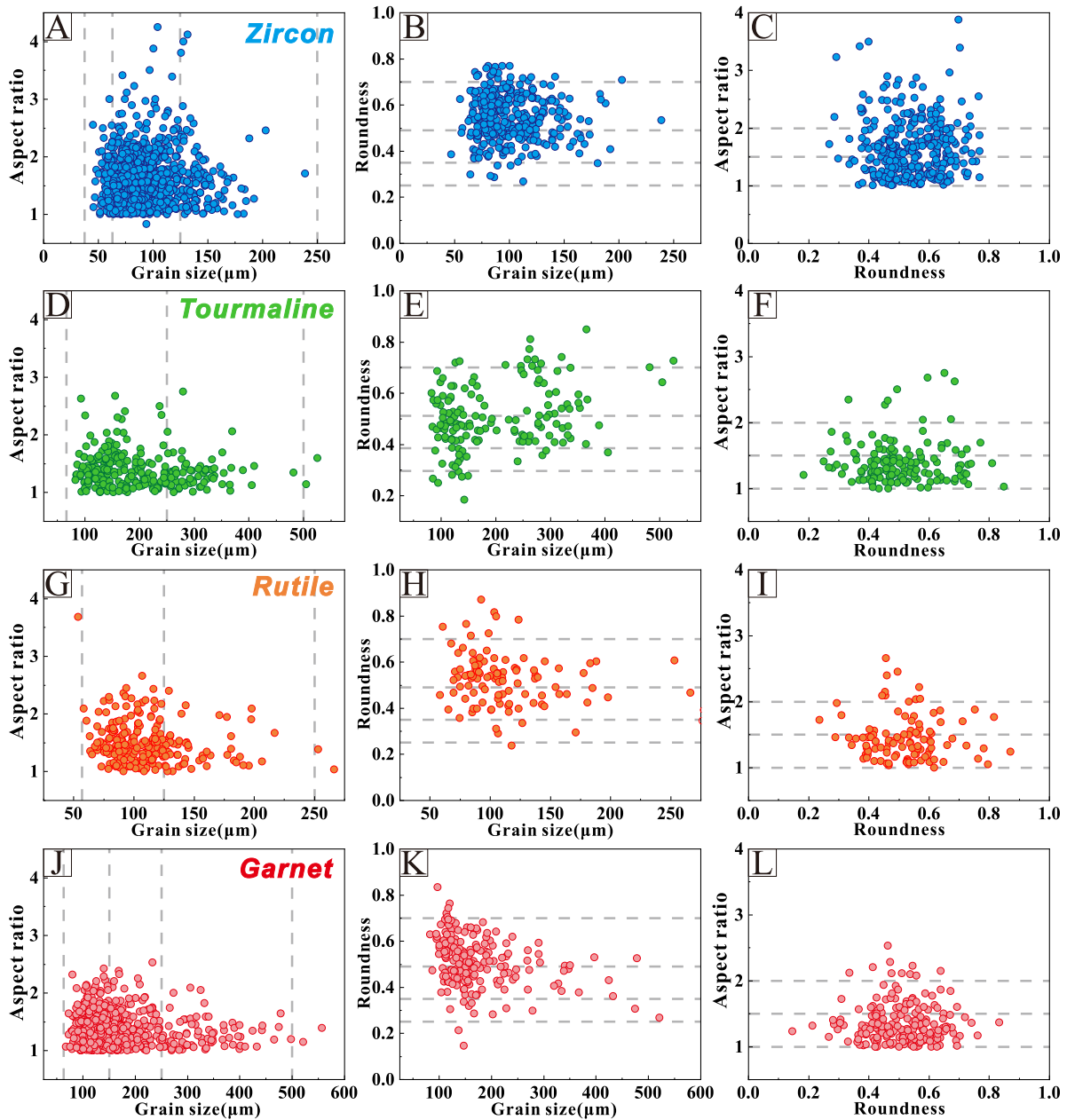


Fig. 4. Textural parameters for analyzed detrital zircon (A–C), tourmaline (D–F), rutile (G–I) and garnet grains (J–L). The gray horizontal lines separated analyzed grains in different grain textural fractions.

granulite-facies and high-grade metamafic rock take 11 % and 10 %, respectively (Table S5). Discrimination using Tolosana-Delgado's method shows that 96 % of grains are from metamorphic rocks with integrated probabilities higher than 50 %. In addition, 28 grains have possibilities of igneous rocks higher than 50 % and no grain is accounted for ultramafic rocks. In 637 metamorphic garnet grains, garnets from amphibolite-facies rocks (B) dominated (86 %) with subordinate granulite-facies (14 %) and only two grains are from eclogite-facies metamorphic rocks (Fig. 10B). The grain size and aspect ratio of all analyzed garnet grains and roundness of 199 grains from five samples were obtained. About 35 % and 53 % of analyzed garnet grains are within 63–125 μm and 125–250 μm , respectively (Figs. 3, 4J). The other 12 % are larger than 250 μm . The aspect ratios of garnet grains are mainly lower than 1.5 (72 %; Fig. 4L). Grains with aspect ratios of 1.5–2 and >2 take 21 % and 7 %, respectively. Analyzed garnet grains are mainly subrounded (35 %) and rounded (50 %; Fig. 4K).

Two discrimination methods indicate that more grains are classified as amphibolite-facies sourced in the >250 μm fraction (91 % and 97 %) compared with 63–125 μm (77 % and 85 %) and 125–250 μm (77 % and 84 %) fractions (Fig. 10A, C). The p-values based on two methods are both lower than 0.05 (Table 2) indicating the parent rock types are related to the grain sizes of detrital garnet. Based on the Mg–Fe²⁺ + Mn–Ca diagram, garnet in the subrounded fraction is composed of 79 % amphibolite-facies sourced and 18 % metamafic rock sourced grains, which is similar with the rounded fraction (75 % amphibolite-facies and 20 % metamafic rocks; Fig. 10B). Discrimination results from Tolosana-Delgado's method also indicate similar contents of two roundness fractions (Fig. 10D). The chi squared test of roundness and aspect ratio with garnet components concludes p-values larger than 0.05 (Table 2). In addition, metamorphic pressure–temperature indicators (Fe²⁺/Mg²⁺ and Mn²⁺/Mg²⁺) indicate a descending trend with decreasing average grain size (Fig. 11).

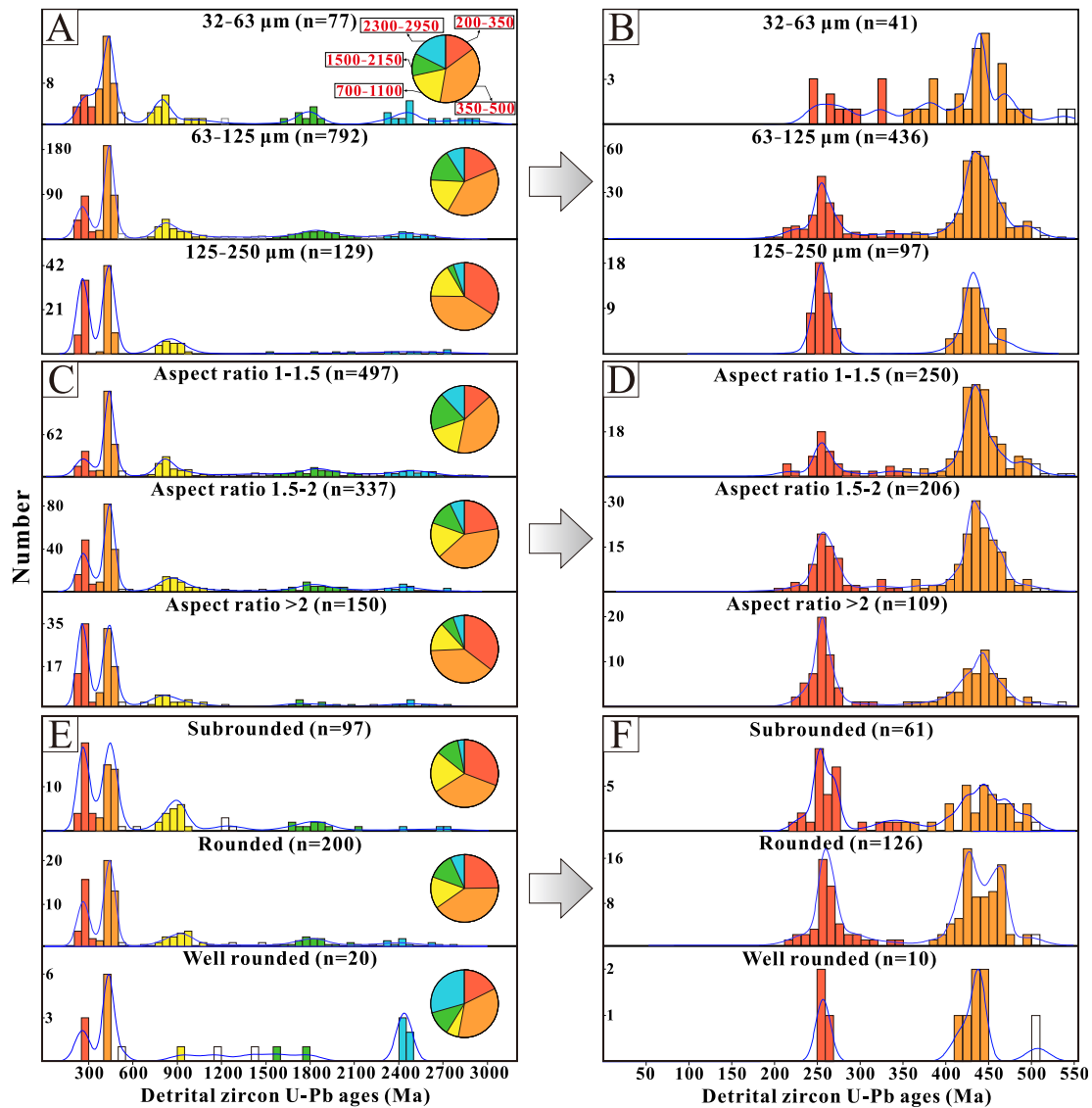


Fig. 5. Detrital zircon U-Pb age populations of different grain size (A, B), aspect ratio (C, D) and roundness (E, F) fractions. Left panels contain all ages and right panels are Phanerozoic ages (Vermeesch, 2012). Bandwidth = 50 Ma. The proportion of different age ranges is shown by pie charts.

5. Discussion

5.1. Inheritance of grain texture features from parent rocks

Our detrital single-mineral analysis results indicate that the northern and eastern Qaidam basin is fed by various rock types, including intermediate-acid rocks, various grades of metamorphic rocks and recycled sedimentary rocks (Figs. 5, 7, 8, 10). Involving the grain texture of detrital mineral grains to their geochronological and geochemical data yielded different correlations. As the initiation of sediments, grain texture (especially grain size and aspect ratio) distribution in parent rocks has a significant impact on the grain texture of grains in sediments (Liang et al., 2023; Feil et al., 2024). Therefore, the influence of inherited grain texture from parent rocks needs first-order considering.

5.1.1. Detrital zircon

Well-marked 350–500 Ma and 200–350 Ma detrital U-Pb age signatures in our samples indicate major contributions from early Paleozoic granitic rocks and Permian–Triassic plutons or siliciclastic sedimentary strata in the Qilian Shan (Wu et al., 2016; Jian et al., 2023). The subordinate Neoproterozoic age (700–1100 Ma) reflects a source of early–mid

metasedimentary basement of the Qilian orogen (Jian et al., 2024). Two Paleoproterozoic age groups (1500–2150 Ma, 2300–2950 Ma) are attributed to the Quanji massif, a crystalline metamorphic basement within the South Qilian–North Qaidam belt (Zhang et al., 2020; Jian et al., 2024). However, combined with the grain textural parameters, we find that two Paleoproterozoic ages are barely preserved in the 125–250 μm fraction (a common size-window in single mineral analysis) and in the aspect ratio > 2 fraction (Fig. 5A, C). Meanwhile, the proportion of two Phanerozoic age groups, as well as the proportion of Permian–Triassic ages in Phanerozoic ages, takes ascending proportions with increasing grain size and increasing aspect ratio (Fig. 5A–D).

The grain texture of mineral grains in parent rocks is related to the crystal system and crystallization environment. One mineral species could have various shapes in host rocks (e.g., different prism and pyramid types of zircon crystals). Zircon crystal is a tetragonal system and commonly develops prism and pyramids, and thus euhedral zircons are columnar with the aspect ratio ranging from 1:1 to >6:1 (Gärtner and Linnemann, 2013). In igneous rocks, the morphology of zircon crystal is related with crystallization temperature and magma chemistry (Pupin, 1980; Belousova et al., 2006). The Al/(Na + K) ratio controls the development of pyramids of zircon crystals and temperature mainly

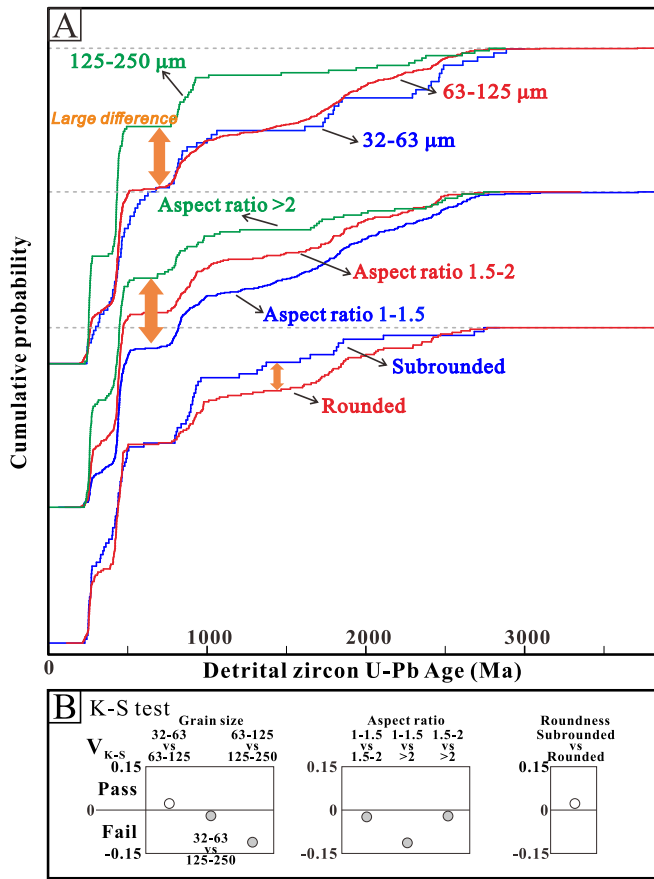


Fig. 6. Detrital zircon U-Pb cumulative age distributions (A). IsoplotR from Vermeesch (2018) is applied for data visualization. Gray dashed lines represent 100%. Dissimilarity between cumulative age distribution curves evaluated by the K-S method (B). Significant difference between two curves is indicated by negative V_{K-S} value (fail; marked by gray circles) and positive value (pass; white circles) represents no significant difference between two distributions.

influences the development of prism (Pupin, 1980). The grain size of zircon is also diverse in different rock types (e.g., zircons in plutons are commonly larger than those in volcanic rocks), and even in different source terranes (Moecher and Samson, 2006). Despite zircon being one of the most stable minerals in chemical and physical weathering and diagenetic processes (Morton and Hallsworth, 2007), the shape of zircon grains could be modified intensively and hardly preserved after

Table 2
Pearson's chi-squared test results of independence between parent rock types of detrital tourmaline, detrital rutile, and detrital garnet and their grain size, roundness and aspect ratio.

Chi-squared test	χ^2	p-Value	Result ^c
<i>Tourmaline</i>			
Grain size	25.97938	0.0000319	Yes
Aspect ratio	0.540168	0.7633	No
Roundness	2.207603	0.3316	No
<i>Rutile</i>			
Grain size	1.9726	0.373	No
Aspect ratio	2.6319	0.2682	No
Roundness	0.3348	0.8459	No
<i>Garnet</i>			
Grain size ^a	12.6183	0.0495	Yes
Grain size ^b	11.2306	0.0241	Yes
Aspect ratio ^a	0.3102	0.9581	No
Aspect ratio ^b	1.6516	0.4379	No
Roundness ^a	0.4547	0.9287	No
Roundness ^b	0.7228	0.6967	No

^a Parent rock lithology discrimination results from Mg-Fe²⁺ + Mn-Ca ternary diagram of Mange and Morton (2007).

^b Parent rock lithology discrimination results from Tolosana-Delgado's method (Tolosana-Delgado et al., 2018).

^c If p-value < 0.05, the null hypothesis (H_0 : the parent rock lithology distribution is independent of grain size) is rejected (annotated by yes); otherwise, the null hypothesis is accepted (annotated by no).

multi-sedimentary cycles. Instead, modifications, since zircon involved into sedimentary systems, have an impact on the shape of zircon grains (Augustsson et al., 2018). Older recycled zircon grains tend to be more rounded and thus to be smaller than younger grains which underwent fewer recycling (Yang et al., 2012; Resentini et al., 2018), even though zircon can develop rims around the core during diagenetic processes. Based on this, we speculate that zircon grains in Paleoproterozoic metasedimentary rocks have originally smaller grain size and lower aspect ratio shape than those in younger Phanerozoic igneous rocks. Consequently, the grain texture of zircon grains in different parent rocks may be a major reason for dependence of grain texture and U-Pb ages.

Our results provide supports for researches which concluded there is a relationship between grain texture and zircon U-Pb ages (e.g., Lawrence et al., 2011; Yang et al., 2012; Castillo et al., 2022) against researches which demonstrate no relationship (e.g., Sircombe and Stern, 2002; Malusà et al., 2013; Muhlbauer et al., 2017). Here, we combined data in this study and from other four studies which provided valuable detrital zircon U-Pb ages and grain size (Sircombe and Stern, 2002; Lawrence et al., 2011; Yang et al., 2012; Malusà et al., 2013). Zircons from modern Yangtze and Amazon river sediments indicate

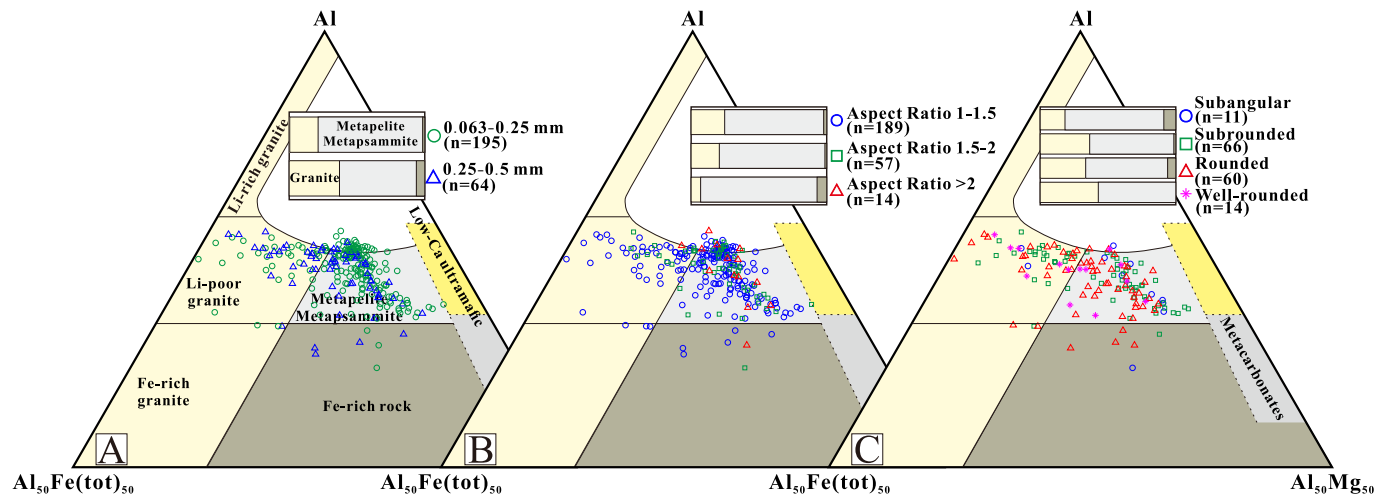


Fig. 7. Major element geochemical data of detrital tourmaline in different grain size (A), aspect ratio (B) and roundness (C) fractions in a discrimination diagram of Henry and Guidotti (1985).

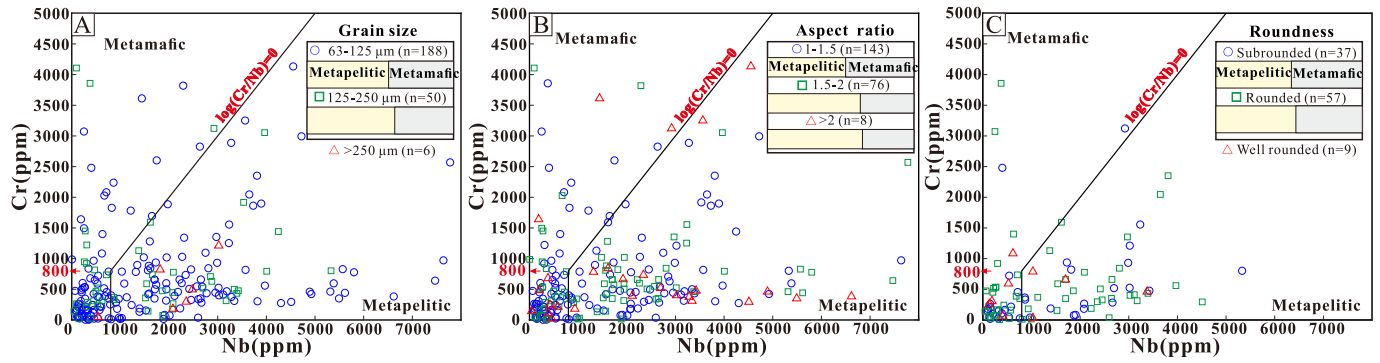


Fig. 8. Detrital rutile Cr–Nb parent rock lithology discrimination following the method of Meinhold et al. (2008). Bar plots show the distribution of parent rocks for different fractions.

descending average grain sizes of detrital zircons as U–Pb ages increase (Fig. 12). However, detrital zircons collected from rivers draining the Slave Craton and European Alps indicate that there is no statistically significant difference between grain size and age populations (Sircombe and Stern, 2002; Malusà et al., 2013). By comparing detrital zircon age populations and grain size in five drainage systems, we note that three grain size-dependent cases show polymodal detrital zircon U–Pb age spectra (i.e., >2 age clusters) and have a relatively wide range of zircon ages (Fig. 12). These features may indicate various sources with diverse ages. Furthermore, in the Cenozoic Qaidam basin and the Yangtze and Amazon catchments, (meta)sedimentary strata serve as important potential sources for detrital zircons (Fig. 2; Yang et al., 2009; Liu et al., 2018; Revels et al., 2021; Fadul et al., 2022; Jian et al., 2024). By contrast, the grain size-independent cases (i.e., the European Alps and the Slave Craton) are characterized by narrow detrital zircon age ranges and less age peaks (Fig. 12), indicating limited sources with similar age (Fig. 12). Therefore, we advocate that grain textural bias in detrital U–Pb ages should be seriously considered in areas which have various sources with diverse ages and especially have contributions from metasedimentary strata (Fig. 13).

5.1.2. Detrital tourmaline

The detrital tourmaline geochemical composition of our sandstone samples reflects contributions from intermediate-acid igneous rocks and metasedimentary rocks in the Qilian Shan (Jian et al., 2013a). However, detrital tourmaline shows variability in different grain size fractions (Fig. 7), which could be supported by the chi squared test (Table 2). Detrital tourmaline from granite takes larger proportions in the 250–500 μm fraction than that in the 63–250 μm fraction (Fig. 7). On the contrary, detrital tourmaline in two major aspect ratio fractions is similar in the composition (Fig. 7).

Tourmaline crystal is a trigonal system and has various morphology in different host rocks (individual or in aggregates), such as prismatic and acicular in metamorphic rocks, columnar and granular in igneous rocks, and needlelike in hydrothermal veins (Kalliomäki et al., 2017; Henry and Dutrow, 2018; Li et al., 2022). Tourmaline in different host rocks also varies in grain size. For example, metamorphic tourmalines from the Archean gold deposits in Finland had a maximum grain size of 250 μm while magmatic tourmalines ranged up to 800 μm in size (Fig. S2; Kalliomäki et al., 2017). Tourmaline grains are found to be finer in metamorphic rocks (60–100 μm) than magmatic rocks

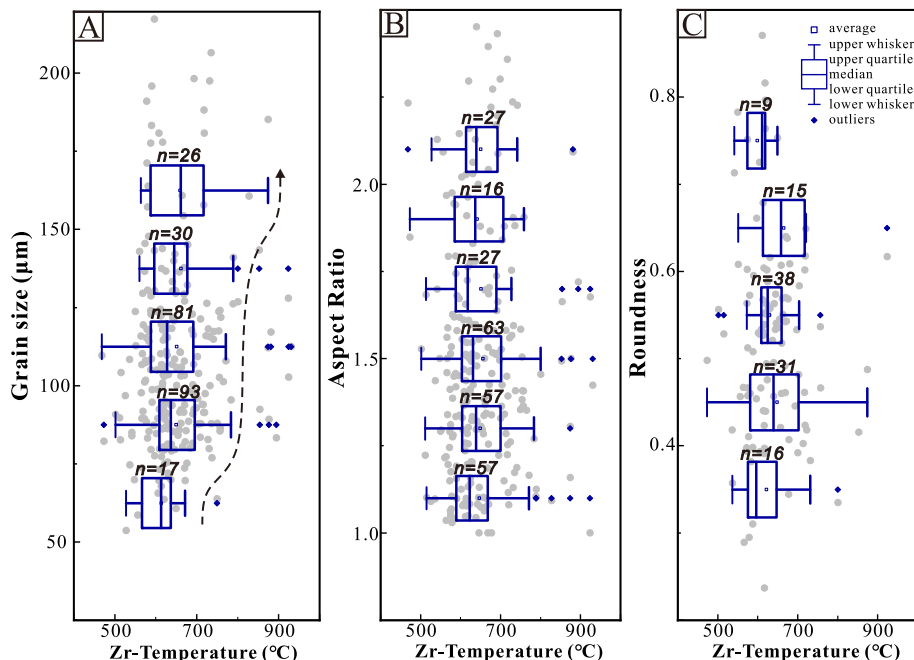


Fig. 9. Relationships between detrital rutile Zr-temperature and grain size (A), aspect ratio (B) and roundness (C).

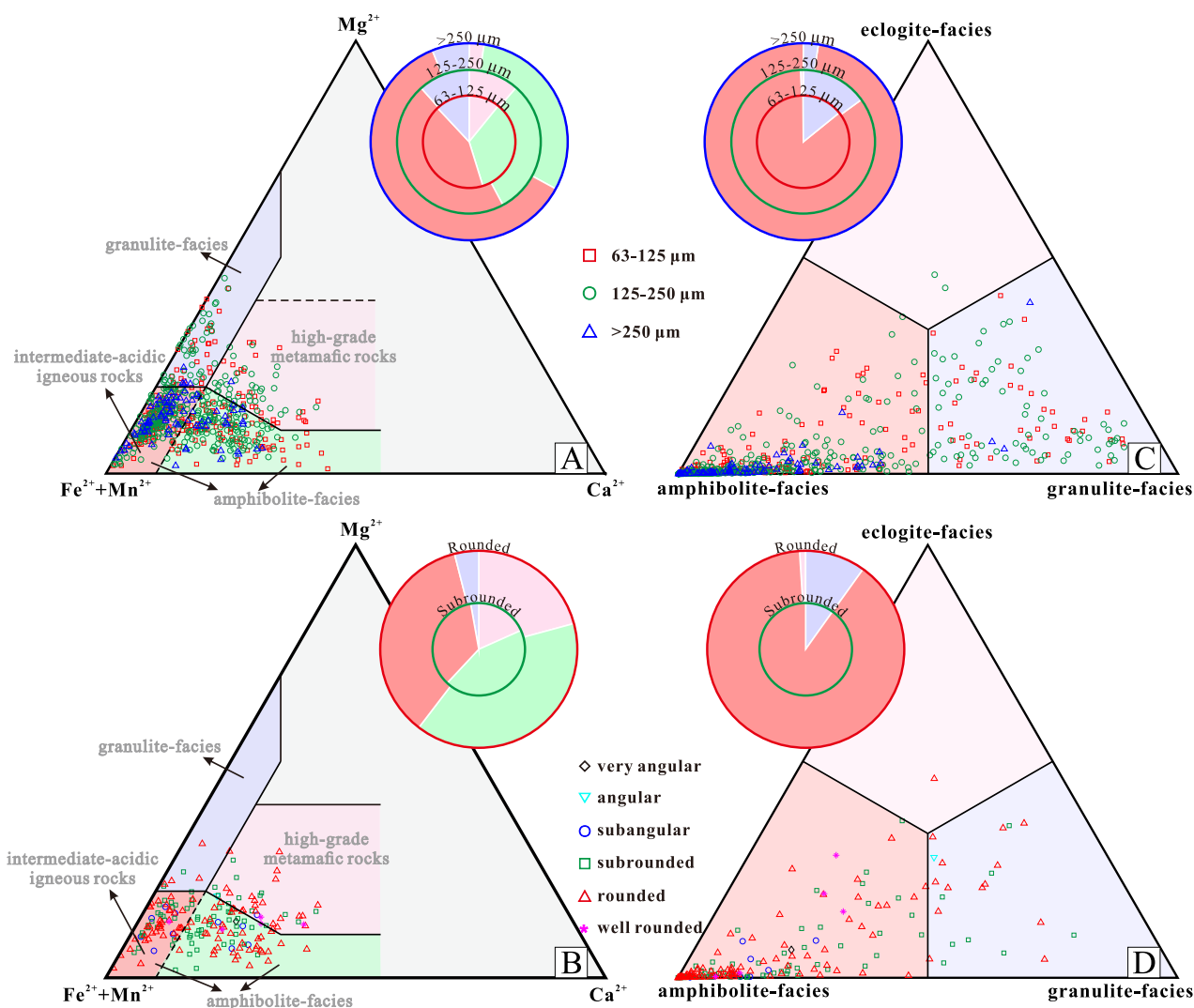


Fig. 10. Parent rock lithology discrimination using detrital garnet major element and relationship between grain size and roundness and parent rock lithology interpretation. Left panels (A–B) are the plot of detrital garnet major element geochemistry of *Mange and Morton (2007)*. Right panels (C–D) are following the discrimination scheme proposed by *Tolosana-Delgado et al. (2018)*. Note that only metamorphic garnets (sum of possibilities of metamorphic-sourced grains larger than 50 %) are plotted.

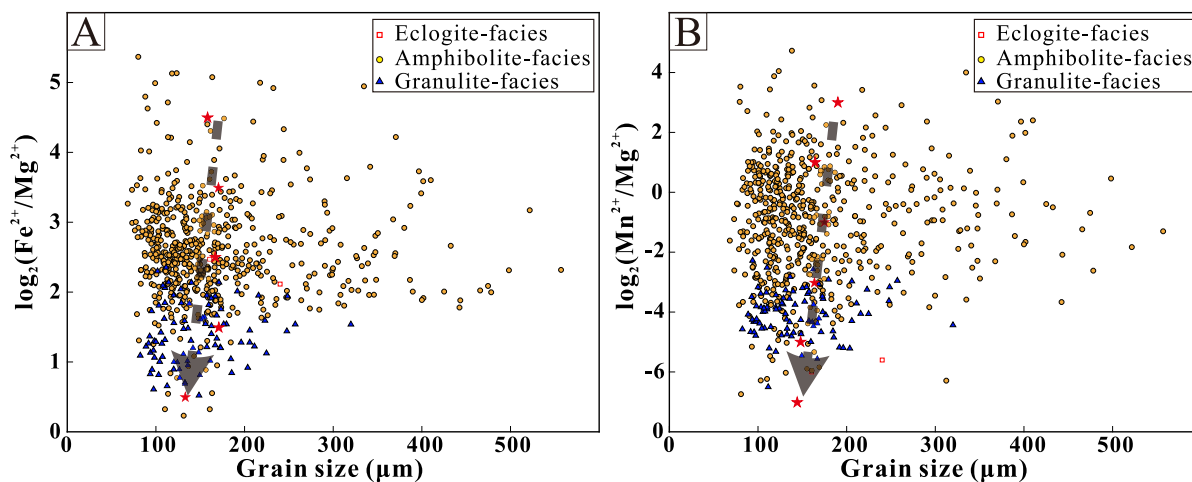


Fig. 11. Grain size vs Fe^{2+}/Mg^{2+} and Mn^{2+}/Mg^{2+} of detrital garnet. Average grain sizes of different ratios (in equal interval) are marked by red stars. The garnet classification is based on the scheme in *Tolosana-Delgado et al. (2018)*.

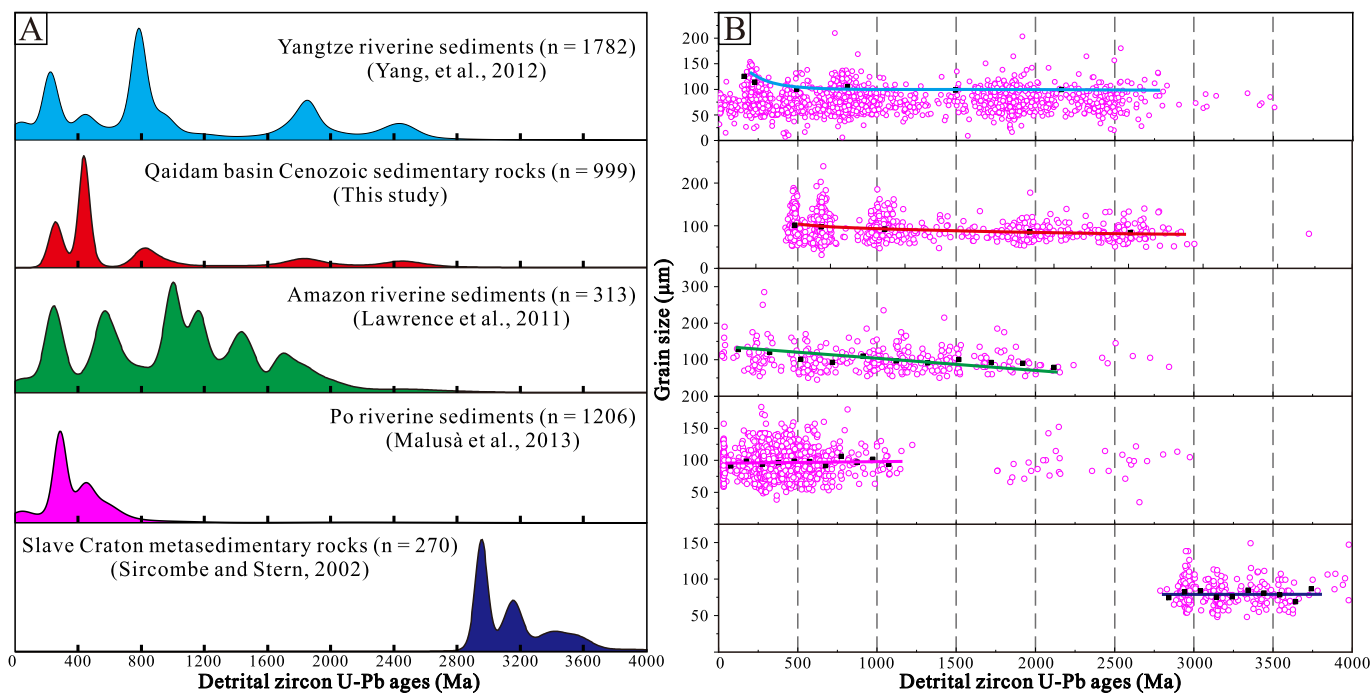


Fig. 12. Detrital zircon U-Pb age distributions (A) and binary plots of detrital zircon grain size and ages (B). Data were collected from Sircombe and Stern (2002), Lawrence et al. (2011), Yang et al. (2012), Malusà et al. (2013), and this study. The black squares are average grain size values. Top three cases represent regions covering various age groups and wide age ranges, and all of them indicate that grain size gets smaller in older grains. Zircon grains in Po River sediments and Slave Craton sedimentary rocks represent a narrow age range and show that zircon age is independent of grain size.

(100–1200 μm) in the Altyn Tagh and Qilian orogenic belts (Fig. S2; Hong et al., 2021; Liu and Jiang, 2021), which are considered as important, potential sediment source terranes for the Cenozoic Qaidam basin. Therefore, we attribute the difference of tourmaline composition in different grain size fractions to the inheritance variation from the parent rocks (Fig. 13). Similar conclusions were drawn in other case investigations. For example, modern sands from the Black Hills indicated that metamorphic tourmalines were dominant in very fine sand and the proportion of granitic tourmalines gradually increased with increasing grain sizes (Viator, 2003).

5.1.3. Detrital rutile

Detrital rutile Cr–Nb contents reveal that both metamafic and metapelitic rocks contribute to the Mesozoic rutile grains (Fig. 8). Based on the chi squared test, rutile composition is found to have no relationship with grain size and aspect ratio (Fig. 8; Table 2). However, the Zr-temperature of detrital rutile displays a certain increasing trend with the grain size (Fig. 9). Rutile is of tetragonal system and is commonly needlelike, fibrous or granular in parent rocks (Meinhold, 2010). As a typical mineral sourced from metamorphic rocks, the grain size of rutile is commonly larger in high-grade metamorphic rocks than those in low- to medium-grade metamorphic rocks (Meinhold, 2010). Therefore, Zr-temperature which indicated metamorphic conditions rather than lithology discrimination based on Cr–Nb contents of detrital rutile is influenced by inherited grain size. No significant relation between the trace element chemistry of detrital rutile and grain size is also shown in sand and sandstone samples investigated by von Eynatten et al. (2005). Despite that, when using detrital rutile geochemistry for parent rock lithology discrimination, common-used size fractions (63–125 and 125–250 μm) are recommended to be optimized toward one single fraction containing the largest amount of rutile in sedimentary studies (Triebold et al., 2012).

5.1.4. Detrital garnet

The major element composition of detrital garnet reveals major sources from amphibolite-facies and granulite-facies metasedimentary rocks in the Qilian Shan (Jian et al., 2013a). Detrital garnet from

amphibolite-facies rocks is much more in both the 63–125 μm fraction and 125–250 μm fraction than that in the >250 μm fraction (Fig. 10), which is also demonstrated by decreasing average grain size with decreasing Fe^{2+}/Mg^{2+} and Mn^{2+}/Mg^{2+} values (Fig. 11). Detrital garnets are commonly granular and have a low aspect ratio range (mostly <2 in this study). The influence of aspect ratio to detrital garnet geochemistry is thus not discussed in this study.

Garnet is a typical cubic system mineral and commonly occurs in parent rocks with regular granular shape, and thus originally has a low aspect ratio. Grain size distribution of garnet in metamorphic rocks is thought to be related to the metamorphic environment where garnet grains crystallize (Krippner et al., 2015; Feil et al., 2024). Commonly, the grain size of garnet is increasing with increasing metamorphic grade (Krippner et al., 2016; Schöning et al., 2018). A reversed trend could also exist, and coarse-grained garnet from lower-grade mica schists was found (Schöning et al., 2021). Grain size variations also occur in garnet grains from igneous rocks. Due to the difference of crystallization processes, garnets from intrusive rocks (e.g., leucogranite) could be much larger (up to a few mm) than that from extrusive rocks (e.g., andesite; up to 100 μm) (Alonso-Perez et al., 2009; Jung et al., 2009). Therefore, the difference of garnet composition between different size fractions may be due to the inheritance variation from the parent rocks. Grain size-dependent patterns are also found in pyrope contents in the Rhine River sediments (Hülscher et al., 2018). Grossular-rich garnets are found to be more frequent in smaller grain sizes while pyrope-rich garnets are more frequent in coarser grain sizes based on the investigation of sedimentary rocks in the central Eastern European Alps (Krippner et al., 2015, 2016).

5.2. Sedimentary environment-induced grain textural bias

Hydrodynamics of sedimentary environments decide the grain texture distribution in the sediment due to the mechanical sedimentary differentiation (Garzanti et al., 2008). For example, alluvial deposit is commonly characterized by coarse-grained sand or conglomerates whereas sediments in lacustrine facies or shallow marine are composed of fine-grained sand or silt. According to the settling-equivalent principle, detrital

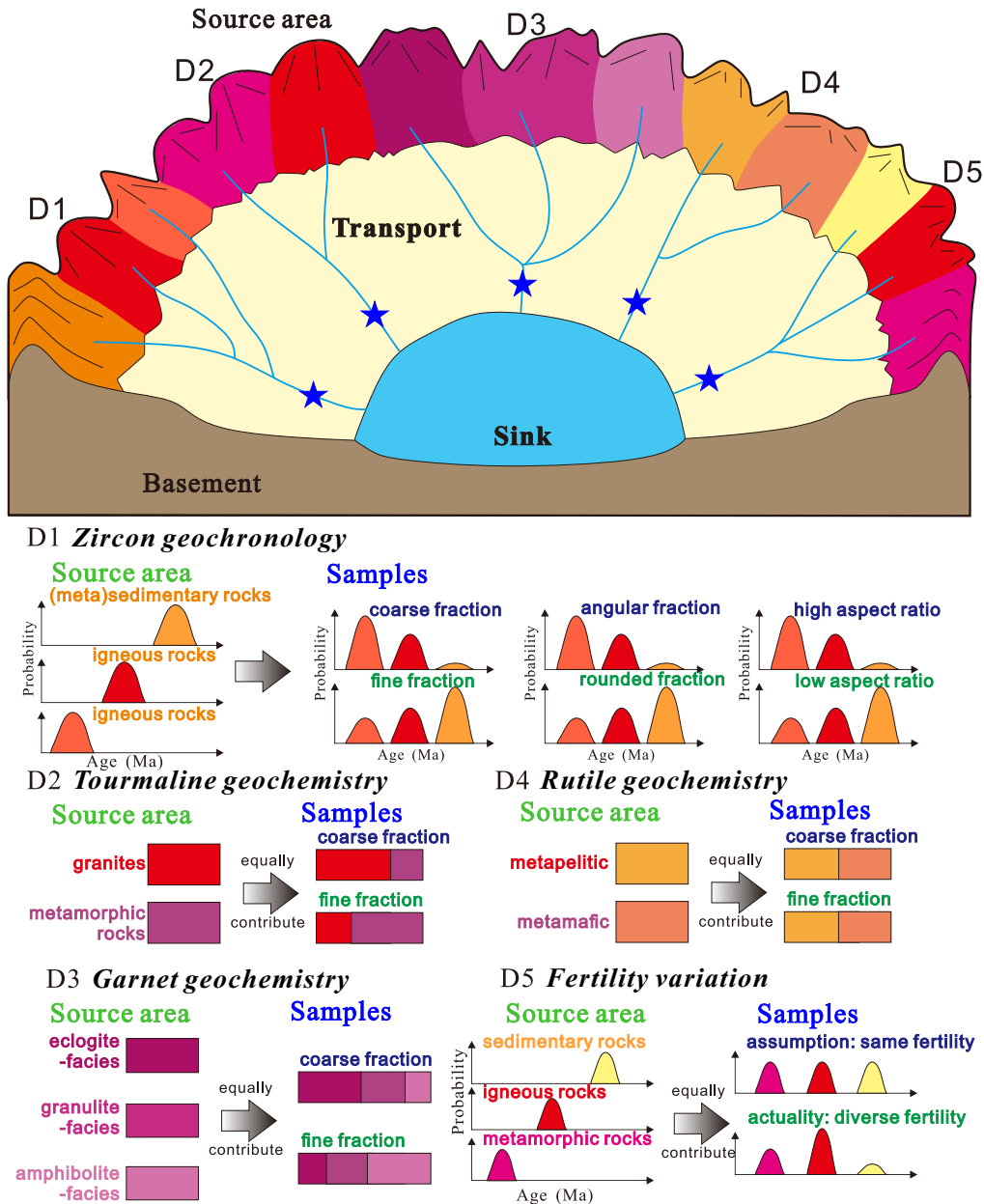


Fig. 13. Schematic diagram of potential textural bias and other biases when using single mineral provenance analysis. Five drainage systems (marked with D*) with different parent rock types are drawn. In each drainage system, it is assumed that each source contributes same sediment flux. Zircon U–Pb geochronology could be influenced by grain texture, especially in regions with contributions from recycled (meta)sedimentary rock (D1). Parent rock discrimination of tourmaline and garnet could be affected by grain size (D2 and D3). Grain textural bias is weak in rutile provenance analysis (D4). In drainage system 5 (D5), take zircon as an example, it is often assumed or ignored that zircon fertility in different rocks is same and each source equally contributes sediments, but the age spectra would be largely different from the actuality which means that zircon fertility in different rocks is largely different (Malusà et al., 2016).

grains are often deposited together with smaller grains of higher density (Rubey, 1933). Despite this physical rules are often used to explain intrasample modal variability, it is reasonable that one specific type of mineral grains with different size or density (even though density of one mineral species usually varies little in density) deposits in different size classes.

As mentioned above, the northern and eastern Qaidam basin experiences a temporal change of the sedimentary environment, from alluvial to fluvial, deltaic and lacustrine to alluvial (Fig. 2; Wang et al., 2023). Our samples collected with different sedimentary facies have a wide range of grain size from fine- to coarse-grained sandstone. The grain size of one specific mineral grain is correlated with the host sand size (Lawrence et al., 2011). Analyzed detrital grains from different samples also vary in grain size (Figs. S3–S5). Single-mineral geochronology and geochemistry also show inter-sample difference (Jian et al., 2013a, 2024). Despite

these variations were interpreted to be contributions from different sources, the sedimentary environment effect on the grain size, thereby geochronological and geochemical difference, could not be negligible. For example, Lawrence et al. (2011) found that zircons from different micro-environments of a single dune present significantly different detrital zircon age spectra. In addition, sedimentary environment difference may be accompanied with the variation of source areas (cf. Fig. 23 of Jian et al., 2024). Sediments in lacustrine or deltaic environments with distal sources may be well mixed and preserved information of multi-sources than those proximal deposits (such as alluvial or fluvial environments).

5.3. Sedimentary recycling-induced grain textural bias

Due to strong durability to mechanical and chemical weathering, zircon, tourmaline, rutile and garnet have potential to survive in multi-

recycling episodes (Morton and Hallsworth, 2007; Garzanti and Andò, 2019). During the transport, deposition and diagenesis in the sedimentary cycle, detrital grains are inevitably suffering mechanical and chemical modifications and thus, tend to be smaller and rounder (Garzanti et al., 2012; Resentini et al., 2018; Castillo et al., 2022). Therefore, recycled grains may have a specific grain texture differing with first-cycle grains.

As mentioned above, our detrital zircon U–Pb geochronology data indicate that U–Pb ages in different grain size fractions and aspect ratio fractions are largely different (Figs. 5C–D, 6). Variation in different roundness fractions occurs but is not significant (Figs. 5E–F, 6). Our results emphasize the recycling effect on the older zircons, which could also be supported by studies in other recycled sedimentary rock-supplied areas (Malusà et al., 2013; Castillo et al., 2022). However, different roundness fractions indicate similar discrimination results, revealing no relationship between roundness, aspect ratio and detrital tourmaline, rutile and garnet element geochemistry (Figs. 7, 8, 10; Table 2). Because it is difficult to recognize recycled grains, we propose two possible reasons: firstly, analyzed grains are first-cycle and are mainly from crystalline rocks in the Qilian Shan rather than recycled sedimentary strata, because of low fertility in the sedimentary rocks and secondly, Permian–Cretaceous sedimentary strata in northern Qilian Mountains which are also supplied by crystalline rocks may play as a recycled source, given that most of analyzed grains are characterized by subrounded and rounded fractions (Figs. 3–4). In other words, in those cases with well-defined parent rocks (involving rock types, forming ages and targeting mineral geochemistry), the influences of sedimentary recycling on detrital grain texture and single-mineral provenance interpretations may be able to be addressed. We expect that, in addition to zircon, sedimentary recycling and related roundness bias might be widely present in geochronology (or thermochronology) data-based stable mineral (e.g., rutile U–Pb geochronology and garnet Sm–Nd geochronology) provenance studies.

5.4. Grain textural bias in the Qaidam basin sandstone provenance analysis and its implications

Massive single-mineral geochronological and geochemical data from sedimentary records in the Qaidam basin or adjacent source areas have been reported in the past decade (Pullen et al., 2011; Bush et al., 2016; McRivette et al., 2019; Jian et al., 2024, references therein). The provenance of the northern and eastern Cenozoic Qaidam basin is still under debate on the contribution of East Kunlun Shan to this region (Bush et al., 2016; Song et al., 2019; Cheng et al., 2021; Jian et al., 2024). The Permian–Triassic ages in the detrital zircon age populations were thought to be an indicator for distinguishing contributions of the unroofing of the Eastern Kunlun Range from the Qilian Shan (e.g., Bush et al., 2016), which is not agreed by some other researches (e.g., Cheng et al., 2017; Song et al., 2019), given the existence of Permian–Triassic plutons in the South Qilian–North Qaidam belt (Wu et al., 2016; Zhang et al., 2020). Jian et al. (2024) further proposed that Paleoproterozoic age is a better indicator of detrital zircon age-based provenance interpretation and advocated that the Cenozoic sandstones were from localized, adjacent source terranes in the Qilian Shan. Combined with the relationship between grain texture and detrital zircon U–Pb ages found in this study, we speculate that absence of Paleoproterozoic ages or overwhelming Permian–Triassic ages in some samples may be influenced by the host sand size. For example, samples L87-09 and YCG-38 are medium sandstone (Table S1) and contain few Paleoproterozoic zircons (cf. Fig. 8 in Jian et al., 2024), while other fine-grained sandstone samples contain a certain number of Paleoproterozoic zircons. Despite all potential parent rocks being discriminated in different grain size fractions based on detrital tourmaline and rutile geochemistry, there are significant differences of proportions of parent rocks between difference grain size fractions. In a quantitative perspective, these differences will affect the quantitative description of the source-to-sink system of the Cenozoic Qaidam (Jian et al., 2013b). Dissimilarly, rutile grains in

different textural fractions indicate similar composition of parent rock types. Provenance interpretation of Mesozoic sandstone based on detrital rutile geochemistry is thus not biased by grain texture. Furthermore, grain textural bias in the Qaidam basin sedimentary provenance analysis could influence the reconstruction of tectonics of the northern Tibetan plateau from the clastic sedimentary perspectives. Overestimated contributions from the East Kunlun Shan to the Qaidam basin deposits may cause misunderstanding of the uplift–erosion history of the East Kunlun Shan and Qilian Shan.

6. Conclusions and perspectives

This study compiles a set of detrital single-mineral geochemical (including tourmaline, rutile and garnet) and geochronological (zircon) data and their quantitative grain textural (grain size, aspect ratio and roundness) data from the Qaidam basin Mesozoic and Cenozoic sedimentary rocks to explore the relationship between grain texture and provenance interpretation based on detrital single-mineral geochronology and geochemistry. Our data demonstrate that detrital zircon U–Pb age is dependent on grain texture, especially grain size and aspect ratio. Dependence of detrital tourmaline and garnet parent rock discrimination and grain size is also statistically proven. On the contrary, roundness and aspect ratio are found to be irrelevant with provenance interpretation of detrital tourmaline and garnet. Parent rock discrimination based on detrital rutile geochemistry is barely influenced by grain texture. We attribute the grain textural bias in detrital zircon, tourmaline and garnet to inheritance from parent rocks. Older zircon grains from recycled metasedimentary rocks tend to be smaller and rounded. Tourmaline and garnet grains in different parent rock types vary in grain size. The sedimentary environment plays as an external controlling factor of detrital grain texture in sediments and may influence the provenance interpretation. Recycling processes improve the roundness of grains but have a limited impact on provenance interpretation. The provenance interpretation of the Cenozoic Qaidam basin is biased by grain texture, especially when using zircon U–Pb geochronology. Older distinguished zircons may be absent in some coarse samples and influence the provenance interpretation. The grain size effect on detrital tourmaline and garnet may influence the quantitative analysis in the Cenozoic Qaidam source-to-sink system. The available data indicate that Mesozoic Qaidam provenance analysis based on detrital rutile is not influenced by grain texture.

This study highlights the underestimated grain textural bias in sedimentary provenance analysis when using detrital single-mineral geochronological and geochemical data (Fig. 13). Those potential biases should be carefully evaluated or eliminated in future works. Artificial influences should be avoided during the laboratory proceedings to reduce the grain textural bias. For deep-time sedimentary records, analyzing samples from the same sedimentary facies or same grain size fractions may reduce misunderstandings. For instance, an Excel-based calculation tool could help for modeling mineral distributions in different size fractions and do benefits for selecting proper analyzed size-window (Resentini et al., 2013). This study highlights the fundamental, prevailing textural biases in single-mineral provenance studies and provides reasonable interpretations. Our findings and recommendations are a key step toward better applications of detrital provenance analysis in earth science studies, especially in the period of big earth data. Given the few concerns about quantitative textural description in the current community, it is appealed that grain texture parameters (grain size, roundness and aspect ratio) should be involved in future single-mineral provenance studies.

CRedit authorship contribution statement

Xiaotian Shen: Writing – review & editing, Writing – original draft, Visualization, Methodology, Formal analysis, Data curation, Conceptualization. **Xing Jian:** Writing – review & editing, Resources, Funding

acquisition, Conceptualization. **Wei Zhang:** Writing – review & editing, Resources, Funding acquisition. **Ping Guan:** Writing – review & editing, Supervision, Resources, Investigation.

Data availability

Data will be made available on request.

Declaration of competing interest

The authors declare that they have no known competing financial interests or personal relationships that could have appeared to influence the work reported in this paper.

Acknowledgments

This study was supported by the Natural Science Foundation of Xiamen, China (No. 3502Z20227006), the National Natural Science Foundation of China (No. 41806052) and Xiamen University Fundamental Research Funds for the Central Universities (No. 20720160114). We would like to thank the PetroChina Qinghai Oil Company for supports during the drilling well sample collections. We also appreciate Hanghai Liang, Xin Huang, Ling Fu, Ziya Zhang, Fan Feng, Ruijuan Liu, Xiaoqing Xie, Shibiao Deng, Yiqiu Jin, Guiming Shu and Fang Ma for their help in field work, lab analysis and data collections. We would like to thank Dr. Carita Augustsson and other two anonymous reviewers for their thorough reviews, as well as to the Editor-in-Chief, Dr. Giorgio Basili for his valuable suggestions.

Appendix A. Supplementary data

Supplementary data to this article can be found online at <https://doi.org/10.1016/j.sedgeo.2024.106731>.

References

- Alonso-Perez, R., Müntener, O., Ulmer, P., 2009. Igneous garnet and amphibole fractionation in the roots of island arcs: experimental constraints on andesitic liquids. *Contributions to Mineralogy and Petrology* 157 (4), 541–558. <https://doi.org/10.1007/s00410-008-0351-8>.
- Andersen, T., 2002. Correction of common lead in U–Pb analyses that do not report 204Pb. *Chemical Geology* 192, 59–79. [https://doi.org/10.1016/S0009-2541\(02\)00195-X](https://doi.org/10.1016/S0009-2541(02)00195-X).
- Andersen, T., Elburg, M.A., Magwaza, B.N., 2019. Sources of bias in detrital zircon geochronology: discordance, concealed lead loss and common lead correction. *Earth-Science Reviews* 197, 102899. <https://doi.org/10.1016/j.earscirev.2019.102899>.
- Augustsson, C., Voigt, T., Bernhart, K., Kreißler, M., Gaupp, R., Gärtner, A., Hofmann, M., Linnemann, U., 2018. Zircon size–age sorting and source-area effect: the German Triassic Buntsandstein Group. *Sedimentary Geology* 375, 218–231. <https://doi.org/10.1016/j.sedgeo.2017.11.004>.
- Bao, J., Song, C., Yang, Y., Fang, X., Meng, Q., Feng, Y., He, P., 2019. Reduced chemical weathering intensity in the Qaidam Basin (NE Tibetan Plateau) during the Late Cenozoic. *Journal of Asian Earth Sciences* 170, 155–165. <https://doi.org/10.1016/j.jseaes.2018.10.018>.
- Belousova, E.A., Griffin, W.L., O'Reilly, S.Y., 2006. Zircon crystal morphology, trace element signatures and Hf isotope composition as a tool for petrogenetic modelling: examples from Eastern Australian granitoids. *Journal of Petrology* 47 (2), 329–353. <https://doi.org/10.1093/ptrology/egi077>.
- Bhatia, R.M., 1983. Plate tectonics and geochemical composition of sandstones. *The Journal of Geology* 91 (6), 611–627. <https://doi.org/10.1086/628815>.
- Bhatia, R.M., Crook, K.A.W., 1986. Trace element characteristics of graywackes and tectonic setting discrimination of sedimentary basins. *Contributions to Mineralogy and Petrology* 92 (2), 181–193. <https://doi.org/10.1007/BF00375292>.
- Blowick, A., Haughton, P., Tyrrell, S., Holbrook, J., Chew, D., Shannon, P., 2019. All mixed up: Pb isotopic constraints on the transit of sands through the Mississippi–Missouri River drainage basin, North America. *Geological Society of America Bulletin* 131 (9–10), 1501–1518. <https://doi.org/10.1130/b35057.1>.
- Bush, M.A., Saylor, J.E., Horton, B.K., Nie, J., 2016. Growth of the Qaidam Basin during Cenozoic exhumation in the northern Tibetan Plateau: inferences from depositional patterns and multiproxy detrital provenance signatures. *Lithosphere* 8 (1), 58–82. <https://doi.org/10.1130/L449.1>.
- Cantine, M.D., Setera, J.B., Vantongerren, J.A., Mwinde, C., Bergmann, K., 2021. Grain size and transport biases in an Eadiaran detrital zircon record. *Journal of Sedimentary Research* 91, 913–928. <https://doi.org/10.2110/jsr.2020.153>.
- Caracciolo, L., 2020. Sediment generation and sediment routing systems from a quantitative provenance analysis perspective: review, application and future development. *Earth-Science Reviews* 209, 103226. <https://doi.org/10.1016/j.earscirev.2020.103226>.
- Caracciolo, L., Ravidà, D.C.G., Chew, D., Janßen, M., Lünsdorf, N.K., Heins, W.A., Stephan, T., Stollhofen, H., 2021. Reconstructing environmental signals across the Permian–Triassic boundary in the SE Germanic Basin: a Quantitative Provenance Analysis (QPA) approach. *Global and Planetary Change* 206, 103631. <https://doi.org/10.1016/j.gloplacha.2021.103631>.
- Castillo, P., Bahlburg, H., Fernandez, R., Fanning, C.M., Berndt, J., 2022. The European continental crust through detrital zircons from modern rivers: testing representativity of detrital zircon U–Pb geochronology. *Earth-Science Reviews* 232, 104145. <https://doi.org/10.1016/j.earscirev.2022.104145>.
- Cawood, P.A., Nemchin, A.A., Freeman, M., Sircombe, K., 2003. Linking source and sedimentary basin: detrital zircon record of sediment flux along a modern river system and implications for provenance studies. *Earth and Planetary Science Letters* 210 (1–2), 259–268. [https://doi.org/10.1016/S0012-821X\(03\)00122-5](https://doi.org/10.1016/S0012-821X(03)00122-5).
- Chayes, F., 1949. A simple point counter for thin-section analysis. *American Mineralogist* 34, 1–11.
- Cheng, F., Jolivet, M., Fu, S., Zhang, C., Zhang, Q., Guo, Z., 2016. Large-scale displacement along the Altyn Tagh Fault (North Tibet) since its Eocene initiation: insight from detrital zircon U–Pb geochronology and subsurface data. *Tectonophysics* 677–678, 261–279. <https://doi.org/10.1016/j.tecto.2016.04.023>.
- Cheng, F., Jolivet, M., Hallot, E., Zhang, D., Zhang, C., Guo, Z., 2017. Tectono-magmatic rejuvenation of the Qaidam craton, northern Tibet. *Gondwana Research* 49, 248–263. <https://doi.org/10.1016/j.gr.2017.06.004>.
- Cheng, F., Jolivet, M., Guo, Z., Wang, L., Zhang, C., Li, X., 2021. Cenozoic evolution of the Qaidam basin and implications for the growth of the northern Tibetan plateau: a review. *Earth-Science Reviews* 220, 103730. <https://doi.org/10.1016/j.earscirev.2021.103730>.
- Chew, D., O'Sullivan, G., Caracciolo, L., Mark, C., Tyrrell, S., 2020. Sourcing the sand: accessory mineral fertility, analytical and other biases in detrital U–Pb provenance analysis. *Earth-Science Reviews* 202, 103093. <https://doi.org/10.1016/j.earscirev.2020.103093>.
- Clift, P.D., Shimizu, N., Layne, G.D., Blusztajn, J., 2001. Tracing patterns of erosion and drainage in the Paleogene Himalaya through ion probe Pb isotope analysis of detrital K-feldspars in the Indus Molasse, India. *Earth and Planetary Science Letters* 188 (3–4), 475–491. [https://doi.org/10.1016/S0012-821X\(01\)00346-6](https://doi.org/10.1016/S0012-821X(01)00346-6).
- Dai, J., Wang, C., Hourigan, J., Santosh, M., 2013. Multi-stage tectono-magmatic events of the Eastern Kunlun Range, northern Tibet: insights from U–Pb geochronology and (U–Th)/He thermochronology. *Tectonophysics* 599, 97–106. <https://doi.org/10.1016/j.tecto.2013.04.005>.
- Deal, E., Venditti, J.G., Benavides, S.J., Bradley, R., Zhang, Q., Kamrin, K., Perron, J.T., 2023. Grain shape effects in bed load sediment transport. *Nature* 613 (7943), 298–302. <https://doi.org/10.1038/s41586-022-05564-6>.
- Deng, K., Yang, S., Li, C., Su, N., Bi, L., Chang, Y.-P., Chang, S.-C., 2017. Detrital zircon geochronology of river sands from Taiwan: implications for sedimentary provenance of Taiwan and its source link with the east China mainland. *Earth-Science Reviews* 164, 31–47. <https://doi.org/10.1016/j.earscirev.2016.10.015>.
- Dickinson, W.R., 1970. Interpreting detrital modes of graywacke and arkose. *Journal of Sedimentary Petrology* 40 (2), 695–707. <https://doi.org/10.1306/74D72018-2B21-11D7-8648000102C1865D>.
- Dickinson, W.R., 1985. Interpreting provenance relations from detrital modes of sandstone. In: Zuffa, G.G. (Ed.), *Provenance of Arenites*. Reidel, Dordrecht, NATO ASI Seriesvol. 148, pp. 333–361.
- Dickinson, W.R., 2008. Impact of differential zircon fertility of granitoid basement rocks in North America on age populations of detrital zircons and implications for granite petrogenesis. *Earth and Planetary Science Letters* 275 (1–2), 80–92. <https://doi.org/10.1016/j.epsl.2008.08.003>.
- Dickinson, W.R., Suckek, C.A., 1979. Plate tectonics and sandstone compositions. *American Association of Petroleum Geologists Bulletin* 63 (12), 2164–2182. <https://doi.org/10.1306/2F9188FB-16CE-11D7-8645000102C1865D>.
- Dröllner, M., Barham, M., Kirkland, C.L., Ware, B., 2021. Every zircon deserves a date: selection bias in detrital geochronology. *Geological Magazine* 158 (6), 1135–1142. <https://doi.org/10.1017/S0016756821000145>.
- Fadul, C.M., Oliveira, P., Val, P., 2022. Ongoing landscape transience in the eastern Amazon Craton consistent with lithologic control of base level. *Earth Surface Processes and Landforms* 47 (13), 3117–3132. <https://doi.org/10.1002/esp.5447>.
- Feil, S., von Eynatten, H., Dunkl, I., Schöning, J., Lünsdorf, N.K., 2024. Inherited grain-size distributions: effect on heavy-mineral assemblages in modern and ancient sediments. *Journal of Geophysical Research: Earth Surface* 129, e2023JF007356. <https://doi.org/10.1029/2023JF007356>.
- Folk, R.L., 1968. *Petrology of Sedimentary Rocks*. Austin. Hemphill Publishing Co., USA (170 pp.).
- Gärtner, A., Linnemann, U., 2013. Morphology of zircon crystal grains in sediments – characteristics, classifications, definitions. *Journal of Central European Geology* 59, 65–73.
- Garzanti, E., Andò, S., 2019. Heavy minerals for junior woodchucks. *Minerals* 9 (3), 148. <https://doi.org/10.3390/min9030148>.
- Garzanti, E., Andò, S., Vezzoli, G., 2008. Settling equivalence of detrital minerals and grain-size dependence of sediment composition. *Earth and Planetary Science Letters* 273 (1–2), 138–151. <https://doi.org/10.1016/j.epsl.2008.06.020>.
- Garzanti, E., Andò, S., Vezzoli, G., 2009. Grain-size dependence of sediment composition and environmental bias in provenance studies. *Earth and Planetary Science Letters* 277 (3–4), 422–432. <https://doi.org/10.1016/j.epsl.2008.11.007>.
- Garzanti, E., Andò, S., Vezzoli, G., Lustrino, M., Boni, M., Vermeesch, P., 2012. Petrology of the Namib Sand Sea: long-distance transport and compositional variability in the wind-displaced Orange Delta. *Earth-Science Reviews* 112 (3–4), 173–189. <https://doi.org/10.1016/j.earscirev.2012.02.008>.
- Garzanti, E., Vermeesch, P., Padoan, M., Resentini, A., Vezzoli, G., Andò, S., 2014. Provenance of passive-margin sand (Southern Africa). *The Journal of Geology* 122 (1), 17–42. <https://doi.org/10.1086/674803>.

- Garzanti, E., Andò, S., Limonta, M., Fielding, L., Najman, Y., 2018. Diagenetic control on mineralogical suites in sand, silt, and mud (Cenozoic Nile Delta): implications for provenance reconstructions. *Earth-Science Reviews* 185, 122–139. <https://doi.org/10.1016/j.earscirev.2018.05.010>.
- Gehrels, G.E., 2014. Detrital zircon U–Pb geochronology applied to tectonics. *Annual Review of Earth and Planetary Sciences* 42 (1), 127–149. <https://doi.org/10.1146/annurev-earth-050212-124012>.
- Gehrels, G.E., Yin, A., Wang, X.-F., 2003. Magmatic history of the northeastern Tibetan Plateau. *Journal of Geophysical Research: Solid Earth* 108 (B9), 2423. <https://doi.org/10.1029/2002jb001876>.
- Griffiths, J.C., 1967. *Scientific Method in Analysis of Sediments*. McGraw-Hill, New York (508 pp.).
- Guo, R., Hu, X., Garzanti, E., Lai, W., Yan, B., Mark, C., 2020. How faithfully do the geochronological and geochemical signatures of detrital zircon, titanite, rutile and monazite record magmatic and metamorphic events? A case study from the Himalaya and Tibet. *Earth-Science Reviews* 201, 103082. <https://doi.org/10.1016/j.earscirev.2020.103082>.
- Guo, R., Hu, X., Garzanti, E., Lai, W., 2021. Boron isotope composition of detrital tourmaline: a new tool in provenance analysis. *Lithos* 400, 106360. <https://doi.org/10.1016/j.lithos.2021.106360>.
- Harel, M.A., Mudd, S.M., Attal, M., 2016. Global analysis of the stream power law parameters based on worldwide ¹⁰Be denudation rates. *Geomorphology* 268, 184–196. <https://doi.org/10.1016/j.geomorph.2016.05.035>.
- He, P., Song, C., Wang, Y., Wang, D., Chen, L., Meng, Q., Fang, X., 2021. Early Cenozoic activated deformation in the Qilian Shan, northeastern Tibetan Plateau: insights from detrital apatite fission-track analysis. *Basin Research* 33, 1731–1748. <https://doi.org/10.1111/bre.12533>.
- Henry, D.J., Dutrow, B.L., 2018. Tourmaline studies through time: contributions to scientific advancements. *Journal of Geosciences* 63 (2), 77–98. <https://doi.org/10.3190/jgeosci.255>.
- Henry, D.J., Guidotti, C.V., 1985. Tourmaline as a petrogenetic indicator mineral: an example from the staurolite-grade metapelites of NW Maine. *American Mineralogist* 70, 1–15.
- Hong, D., Jian, X., Fu, L., Zhang, W., 2020. Garnet trace element geochemistry as a sediment provenance indicator: an example from the Qaidam basin, northern Tibet. *Marine and Petroleum Geology* 116, 104316. <https://doi.org/10.1016/j.marpetgeo.2020.104316>.
- Hong, T., Zhai, M.-G., Xu, X.-W., Li, H., Wu, C., Ma, Y.-C., Niu, L., Ke, Q., Wang, C., 2021. Tourmaline and quartz in the igneous and metamorphic rocks of the Tashisayi granitic batholith, Altyn Tagh, northwestern China: geochemical variability constraints on metallogenesis. *Lithos* 400–401, 106538. <https://doi.org/10.1016/j.lithos.2021.106538>.
- Hu, X., Garzanti, E., Wang, J., Huang, W., An, W., Webb, A., 2016. The timing of India–Asia collision onset—facts, theories, controversies. *Earth-Science Reviews* 160, 264–299. <https://doi.org/10.1016/j.earscirev.2016.07.014>.
- Hu, P., Zhai, Q., Cawood, P.A., Weinberg, R.F., Zhao, G., Tang, Y., Liu, Y., 2023. Paleogeographic reconstruction of Precambrian terranes reworked by Phanerozoic orogens: an example based on detrital zircon REE from Lhasa terrane in southern Tibet. *Geophysical Research Letters* 50 (5), e2023GL102979. <https://doi.org/10.1029/2023GL102979>.
- Huang, H., Niu, Y., Nowell, G., Zhao, Z., Yu, X., Zhu, D.-C., Mo, X., Ding, S., 2014. Geochemical constraints on the petrogenesis of granitoids in the East Kunlun Orogenic belt, northern Tibetan Plateau: implications for continental crust growth through syn-collisional felsic magmatism. *Chemical Geology* 370, 1–18. <https://doi.org/10.1016/j.chemgeo.2014.01.010>.
- Hülscher, J., Bahlburg, H., Pfänder, J., 2018. New geochemical results indicate a non-alpine provenance for the Alpine Spectrum (epidote, garnet, hornblende) in quaternary Upper Rhine sediment. *Sedimentary Geology* 375, 134–144. <https://doi.org/10.1016/j.sedgeo.2018.02.010>.
- Jian, X., Guan, P., Zhang, D.-W., Zhang, W., Feng, F., Liu, R.-J., Lin, S.-D., 2013a. Provenance of Tertiary sandstone in the northern Qaidam basin, northeastern Tibetan Plateau: integration of framework petrography, heavy mineral analysis and mineral chemistry. *Sedimentary Geology* 290, 109–125. <https://doi.org/10.1016/j.sedgeo.2013.03.010>.
- Jian, X., Guan, P., Zhang, W., Feng, F., 2013b. Geochemistry of Mesozoic and Cenozoic sediments in the northern Qaidam basin, northeastern Tibetan Plateau: implications for provenance and weathering. *Chemical Geology* 360–361, 74–88. <https://doi.org/10.1016/j.chemgeo.2013.10.011>.
- Jian, X., Guan, P., Zhang, W., Liang, H., Feng, F., Fu, L., 2018. Late Cretaceous to early Eocene deformation in the northern Tibetan Plateau: detrital apatite fission track evidence from northern Qaidam basin. *Gondwana Research* 60, 94–104. <https://doi.org/10.1016/j.gr.2018.04.007>.
- Jian, X., Weislogel, A., Pullen, A., Shang, F., 2020. Formation and evolution of the Eastern Kunlun Range, northern Tibet: evidence from detrital zircon U–Pb geochronology and Hf isotopes. *Gondwana Research* 83, 63–79. <https://doi.org/10.1016/j.gr.2020.01.015>.
- Jian, X., Fu, L., Wang, P., Guan, P., Zhang, W., Fu, H., Mei, H., 2023. Sediment provenance of the Lulehe Formation in the Qaidam basin: insight to initial Cenozoic deposition and deformation in northern Tibetan plateau. *Basin Research* 35 (1), 271–294. <https://doi.org/10.1111/bre.12712>.
- Jian, X., Guan, P., Fu, L., Zhang, W., Shen, X., Fu, H., Wang, L., 2024. Detrital zircon geochronology and provenance of Cenozoic deposits in the Qaidam basin, northern Tibetan plateau: an overview with new data, implications and perspectives. *Marine and Petroleum Geology* 159, 106566. <https://doi.org/10.1016/j.marpetgeo.2023.106566>.
- Johnsson, M.J., 1993. The system controlling the composition of clastic sediments. In: Johnsson, M.J., Basu, A. (Eds.), *Processes Controlling the Composition of Clastic Sediments*. Geological Society of America, Special Paper 284, pp. 1–19.
- Jung, C., Jung, S., Nebel, O., Hellebrand, E., Masberg, P., Hoffer, E., 2009. Fluid-present melting of meta-igneous rocks and the generation of leucogranites—constraints from garnet major- and trace element data, Lu–Hf whole rock–garnet ages and whole rock Nd–Sr–Hf–O isotope data. *Lithos* 111 (3–4), 220–235. <https://doi.org/10.1016/j.lithos.2008.11.008>.
- Kalliomäki, H., Wagner, T., Fusswinkel, T., Sakellaris, G., 2017. Major and trace element geochemistry of tourmalines from Archean orogenic gold deposits: proxies for the origin of gold mineralizing fluids? *Ore Geology Reviews* 91, 906–927. <https://doi.org/10.1016/j.oregeorev.2017.08.014>.
- Krippner, A., Meinhold, G., Morton, A.C., Russell, E., von Eynatten, H., 2015. Grain-size dependence of garnet composition revealed by provenance signatures of modern stream sediments from the western Hohe Tauern (Austria). *Sedimentary Geology* 321, 25–38. <https://doi.org/10.1016/j.sedgeo.2015.03.002>.
- Krippner, A., Meinhold, G., Morton, A.C., Schöning, J., von Eynatten, H., 2016. Heavy minerals and garnet geochemistry of stream sediments and bedrocks from the Almklovdalen area, Western Gneiss Region, SW Norway: implications for provenance analysis. *Sedimentary Geology* 336, 96–105. <https://doi.org/10.1016/j.sedgeo.2015.09.009>.
- Lawrence, R.L., Cox, R., Mapes, R.W., Coleman, D.S., 2011. Hydrodynamic fractionation of zircon age populations. *Geological Society of America Bulletin* 123 (1–2), 295–305. <https://doi.org/10.1130/b30151.1>.
- Leary, R.J., Smith, M.E., Umhoefer, P., 2020. Grain-size control on detrital zircon cyclopropanance in the Late Paleozoic Paradox and Eagle Basins, USA. *Journal of Geophysical Research: Solid Earth* 125 (7), e2019JB019226. <https://doi.org/10.1029/2019jb019226>.
- Li, W., Cao, S., Nakamura, E., Ota, T., Liu, Z., Dong, Y., Kunihiro, T., 2022. Magmatic-hydrothermal processes of the Laojunshan metamorphic massif in Southeastern Asia: evidence from chemical and B-isotopic variations of deformed tourmalines. *Lithos* 412, 106609. <https://doi.org/10.1016/j.lithos.2022.106609>.
- Liang, W., Hu, X., Garzanti, E., Dong, X., Zhang, Y., 2023. Fluvial–aeolian interaction and compositional variability in the river-fed Yarlung Tsangpo Dune System (Southern Tibet). *Journal of Geophysical Research: Earth Surface* 128, e2022JF006920. <https://doi.org/10.1029/2022JF006920>.
- Liu, T., Jiang, S.-Y., 2021. Multiple generations of tourmaline from Yushishanxi leucogranite in South Qilian of western China record a complex formation history from B-rich melt to hydrothermal fluid. *American Mineralogist* 106 (6), 994–1008. <https://doi.org/10.2138/am-2021-7473>.
- Liu, X., Li, A., Dong, J., Lu, J., Huang, J., Wan, S., 2018. Provenance discrimination of sediments in the Zhejiang–Fujian mud belt, East China Sea: implications for the development of the mud depocenter. *Journal of Asian Earth Sciences* 151, 1–15. <https://doi.org/10.1016/j.jseas.2017.10.017>.
- Lu, H., Ye, J., Guo, L., Pan, J., Xiong, S., Li, H., 2019. Towards a clarification of the provenance of Cenozoic sediments in the northern Qaidam Basin. *Lithosphere* 11 (2), 252–272. <https://doi.org/10.1130/l1037.1>.
- Malusà, M.G., Zattin, M., Andò, S., Garzanti, E., Vezzoli, G., 2009. Focused erosion in the Alps constrained by fission-track ages on detrital apatites. *Geological Society, London, Special Publications* 324 (1), 141–152. <https://doi.org/10.1144/sp324.11>.
- Malusà, M.G., Carter, A., Limoncelli, M., Villa, I.M., Garzanti, E., 2013. Bias in detrital zircon geochronology and thermochronometry. *Chemical Geology* 359, 90–107. <https://doi.org/10.1016/j.chemgeo.2013.09.016>.
- Malusà, M.G., Resentini, A., Garzanti, E., 2016. Hydraulic sorting and mineral fertility bias in detrital geochronology. *Gondwana Research* 31, 1–19. <https://doi.org/10.1016/j.gr.2015.09.002>.
- Mange, M.A., Morton, A.C., 2007. Geochemistry of heavy minerals. In: Mange, M.A., Wright, D.T. (Eds.), *Heavy Minerals in Use: Developments in Sedimentology* vol. 58, pp. 345–391. [https://doi.org/10.1016/s0070-4571\(07\)58013-1](https://doi.org/10.1016/s0070-4571(07)58013-1).
- Mattinson, C.G., Menold, C.A., Zhang, J.X., Bird, D.K., 2010. High- and ultrahigh-pressure metamorphism in the North Qaidam and South Altyn Terranes, Western China. *International Geology Review* 49 (11), 969–995. <https://doi.org/10.2747/0020-6814.49.11.969>.
- McBride, E.F., 1963. A classification of common sandstones. *Journal of Sedimentary Petrology* 33, 664–669.
- McLennan, S.M., Hemming, S., McDaniel, D.K., Hanson, G.N., 1993. *Geochemical approaches to sedimentation, provenance, and tectonics*. In: Johnsson, M.J., Basu, A. (Eds.), *Processes Controlling the Composition of Clastic Sediments* Special Paper Geological Society of America vol. 284, pp. 21–40.
- McRivette, M.W., Yin, A., Chen, X., Gehrels, G.E., 2019. Cenozoic basin evolution of the central Tibetan plateau as constrained by U–Pb detrital zircon geochronology, sandstone petrology, and fission-track thermochronology. *Tectonophysics* 751, 150–179. <https://doi.org/10.1016/j.tecto.2018.12.015>.
- Meinhold, G., 2010. Rutile and its applications in earth sciences. *Earth-Science Reviews* 102 (1–2), 1–28. <https://doi.org/10.1016/j.earscirev.2010.06.001>.
- Meinhold, G., Anders, B., Kostopoulos, D., Reischmann, T., 2008. Rutile chemistry and thermometry as provenance indicator: an example from Chios Island, Greece. *Sedimentary Geology* 203 (1–2), 98–111. <https://doi.org/10.1016/j.sedgeo.2007.11.004>.
- Moehler, D., Samson, S., 2006. Differential zircon fertility of source terranes and natural bias in the detrital zircon record: implications for sedimentary provenance analysis. *Earth and Planetary Science Letters* 247 (3–7), 252–266. <https://doi.org/10.1016/j.epsl.2006.04.035>.
- Morton, A.C., 1985. A new approach to provenance studies: electron microprobe analysis of detrital garnets from Middle Jurassic sandstones of the northern North Sea. *Sedimentology* 32, 553–566. <https://doi.org/10.1111/j.1365-3091.1985.tb00470.x>.
- Morton, A.C., 1991. Geochemical studies of detrital heavy minerals and their application to provenance research. *Geological Society, London, Special Publications* 57 (1), 31–45. <https://doi.org/10.1144/gsl.sp.1991.057.01.04>.
- Morton, A.C., Hallsworth, C., 2007. Stability of detrital heavy minerals during burial diagenesis. In: Mange, M.A., Wright, D.T. (Eds.), *Heavy Minerals in Use: Developments in Sedimentology* [https://doi.org/10.1016/s0070-4571\(07\)58007-6](https://doi.org/10.1016/s0070-4571(07)58007-6) (215–245 pp.).

- Morton, A.C., Whitham, A.G., Fanning, C.M., 2005. Provenance of Late Cretaceous to Paleocene submarine fan sandstones in the Norwegian Sea: integration of heavy mineral, mineral chemical and zircon age data. *Sedimentary Geology* 182 (1–4), 3–28. <https://doi.org/10.1016/j.sedgeo.2005.08.007>.
- Muhlbauer, J.G., Fedo, C.M., Farmer, G.L., 2017. Influence of textural parameters on detrital-zircon age spectra with application to provenance and paleogeography during the Ediacaran–Terreneuvian of southwestern Laurentia. *Geological Society of America Bulletin* 129 (11–12), 1585–1601. <https://doi.org/10.1130/B31611.1>.
- Nie, J., Horton, B.K., Saylor, J.E., Mora, A., Mange, M., Garzzone, C.N., Basu, A., Moreno, C.J., Caballero, V., Parra, M., 2012. Integrated provenance analysis of a convergent retroarc foreland system: U–Pb ages, heavy minerals, Nd isotopes, and sandstone compositions of the Middle Magdalena Valley basin, northern Andes, Colombia. *Earth-Science Reviews* 110 (1–4), 111–126. <https://doi.org/10.1016/j.earscirev.2011.11.002>.
- Pettjohn, F.J., Potter, P.E., Siever, R., 1987. *Sand and Sandstone*. 2nd edition. Springer, New York (553 pp.).
- Pullen, A., Kapp, P., McCallister, A.T., Chang, H., Gehrels, G.E., Garzzone, C.N., Heermance, R.V., Ding, L., 2011. Qaidam Basin and northern Tibetan Plateau as dust sources for the Chinese Loess Plateau and paleoclimatic implications. *Geology* 39 (11), 1031–1034. <https://doi.org/10.1130/G32296.1>.
- Pupin, J.P., 1980. *Zircon and granite petrology*. *Contributions to Mineralogy and Petrology* 73, 207–220.
- Resentini, A., Malusà, M.G., Garzanti, E., 2013. MinSORTING: an Excel worksheet for modelling mineral grain-size distribution in sediments, with application to detrital geochronology and provenance studies. *Computers & Geosciences* 59, 90–97. <https://doi.org/10.1016/j.cageo.2013.05.015>.
- Resentini, A., Goren, L., Castellort, S., Garzanti, E., 2017. Partitioning sediment flux by provenance and tracing erosion patterns in Taiwan. *Journal of Geophysical Research: Earth Surface* 122 (7), 1430–1454. <https://doi.org/10.1002/2016jf004026>.
- Resentini, A., Andò, S., Garzanti, E., 2018. Quantifying roundness of detrital minerals by image analysis: sediment transport, shape effects, and provenance implications. *Journal of Sedimentary Research* 88 (2), 276–289. <https://doi.org/10.2110/jgsr.2018.12>.
- Revels, B.N., Rickli, J., Moura, C.A.V., Vance, D., 2021. The riverine flux of molybdenum and its isotopes to the ocean: weathering processes and dissolved-particulate partitioning in the Amazon basin. *Earth and Planetary Science Letters* 559, 116773. <https://doi.org/10.1016/j.epsl.2021.116773>.
- Rieser, A.B., Newbauer, F., Liu, Y., Ge, X., 2005. Sandstone provenance of north-western sectors of the intracontinental Cenozoic Qaidam basin, western China: tectonic vs. climatic control. *Sedimentary Geology* 177 (1–2), 1–18. <https://doi.org/10.1016/j.sedgeo.2005.01.012>.
- Ritts, B.D., Biffi, U., 2001. Mesozoic northeast Qaidam basin: response to contractional reactivation of the Qilian Shan, and implications for the extent of Mesozoic intracontinental deformation in central Asia. *Geological Society of America Memoirs* 194, 293–316.
- Rubey, W.W., 1933. The size-distribution of heavy minerals within a water-laid sandstone. *Journal of Sedimentary Petrology* 3 (1), 3–29.
- Schöning, J., Meinhold, G., von Eynatten, H., Lünsdorf, N.K., 2018. Provenance information recorded by mineral inclusions in detrital garnet. *Sedimentary Geology* 376, 32–49. <https://doi.org/10.1016/j.sedgeo.2018.07.009>.
- Schöning, J., von Eynatten, H., Tolosana-Delgado, R., Meinhold, G., 2021. Garnet major-element composition as an indicator of host-rock type: a machine learning approach using the random forest classifier. *Contributions to Mineralogy and Petrology* 176, 1–21. <https://doi.org/10.1007/s00410-021-01854-w>.
- Sircombe, K.N., Stern, R.A., 2002. An investigation of artificial biasing in detrital zircon U–Pb geochronology due to magnetic separation in sample preparation. *Geochimica et Cosmochimica Acta* 66 (13), 2379–2397. [https://doi.org/10.1016/S0016-7037\(02\)00839-6](https://doi.org/10.1016/S0016-7037(02)00839-6).
- Song, S., Su, L., Niu, Y., Zhang, L., Zhang, G., 2007. Petrological and geochemical constraints on the origin of garnet peridotite in the North Qaidam ultrahigh-pressure metamorphic belt, northwestern China. *Lithos* 96 (1–2), 243–265. <https://doi.org/10.1016/j.lithos.2006.09.017>.
- Song, S., Niu, Y., Su, L., Xia, X., 2013. Tectonics of the North Qilian orogen, NW China. *Gondwana Research* 23 (4), 1378–1401. <https://doi.org/10.1016/j.gr.2012.02.004>.
- Song, S., Niu, Y., Su, L., Zhang, C., Zhang, L., 2014. Continental orogenesis from ocean subduction, continent collision/subduction, to orogen collapse, and orogen recycling: the example of the North Qaidam UHPM belt, NW China. *Earth-Science Reviews* 129, 59–84. <https://doi.org/10.1016/j.earscirev.2013.11.010>.
- Song, B., Zhang, K., Hou, Y., Ji, J., Wang, J., Yang, Y., Yang, T., Wang, C., Shen, T., 2019. New insights into the provenance of Cenozoic strata in the Qaidam Basin, northern Tibet: constraints from combined U–Pb dating of detrital zircons in recent and ancient fluvial sediments. *Palaeogeography, Palaeoclimatology, Palaeoecology* 533, 109254. <https://doi.org/10.1016/j.palaeo.2019.109254>.
- Sorby, H.C., 1880. On the structure and origin of non-calcareous stratified rocks. *Quarterly Journal of the Geological Society of London* 36, 46–92.
- Sun, X., Kuiper, K.F., Tian, Y., Li, C., Zhang, Z., Gemignani, L., Guo, R., de Brij, V.H.L., Wijbrans, J.R., 2020. $^{40}\text{Ar}/^{39}\text{Ar}$ mica dating of late Cenozoic sediments in SE Tibet: implications for sediment recycling and drainage evolution. *Journal of the Geological Society* 177 (4), 843–854. <https://doi.org/10.1144/jgs2019-099>.
- Taylor, S.R., McLennan, S.M., 1995. The geochemical evolution of the continental crust. *Reviews of Geophysics* 33 (2), 241–265. <https://doi.org/10.1029/95RG00262>.
- Tolosana-Delgado, R., von Eynatten, H., Krippner, A., Meinhold, G., 2018. A multivariate discrimination scheme of detrital garnet chemistry for use in sedimentary provenance analysis. *Sedimentary Geology* 375, 14–26. <https://doi.org/10.1016/j.sedgeo.2017.11.003>.
- Tomkins, H.S., Powell, R., Ellis, D.J., 2007. The pressure dependence of the zirconium-in-rutile thermometer. *Journal of Metamorphic Geology* 25 (6), 703–713. <https://doi.org/10.1111/j.1525-1314.2007.00724.x>.
- Triantafyllou, A., Ducea, M.N., Jepson, G., Hernández-Montenegro, J.D., Bisch, A., Ganne, J., 2023. Europium anomalies in detrital zircons record major transitions in Earth geodynamics at 2.5 Ga and 0.9 Ga. *Geology* 51, 141–145. <https://doi.org/10.1130/g50720.1>.
- Triebold, S., von Eynatten, H., Zack, T., 2012. A recipe for the use of rutile in sedimentary provenance analysis. *Sedimentary Geology* 282, 268–275. <https://doi.org/10.1016/j.sedgeo.2012.09.008>.
- Vermeesch, P., 2004. How many grains are needed for a provenance study? *Earth and Planetary Science Letters* 224 (3–4), 441–451. <https://doi.org/10.1016/j.epsl.2004.05.037>.
- Vermeesch, P., 2012. On the visualisation of detrital age distributions. *Chemical Geology* 312–313, 190–194. <https://doi.org/10.1016/j.chemgeo.2012.04.021>.
- Vermeesch, P., 2013. Multi-sample comparison of detrital age distributions. *Chemical Geology* 341, 140–146. <https://doi.org/10.1016/j.chemgeo.2013.01.010>.
- Vermeesch, P., 2018. IsoplotR: a free and open toolbox for geochronology. *Geoscience Frontiers* 9 (5), 1479–1493. <https://doi.org/10.1016/j.gsf.2018.04.001>.
- Viator, 2003. *Detrital Tourmaline as an Indicator of Provenance: A Chemical and Sedimentological Study of Modern Sands From the Black Hills, South Dakota*. Louisiana State University (Master's Theses).
- von Eynatten, H., Dunkl, I., 2012. Assessing the sediment factory: the role of single grain analysis. *Earth-Science Reviews* 115 (1–2), 97–120. <https://doi.org/10.1016/j.earscirev.2012.08.001>.
- von Eynatten, H., Tolosana-Delgado, R., Triebold, S., Zack, T., 2005. Interactions between grain size and composition of sediments: two examples. In: Mateu-Figueras, G., Barcelò-Vidl, C. (Eds.), *Proceedings CoDaWork'05 – 2nd Compositional Data Analysis Workshop S2–4* (1–12 pp., Girona).
- von Eynatten, H., Tolosana-Delgado, R., Karius, V., 2012. Sediment generation in modern glacial settings: grain-size and source-rock control on sediment composition. *Sedimentary Geology* 280, 80–92. <https://doi.org/10.1016/j.sedgeo.2012.03.008>.
- Wadell, H., 1932. Volume, shape and roundness of rock particles. *Journal of Geology* 40, 443–451.
- Wang, L., Jian, X., Fu, H., Zhang, W., Shang, F., Fu, L., 2023. Decoupled local climate and chemical weathering intensity of fine-grained siliciclastic sediments from a paleo-megalake: an example from the Qaidam basin, northern Tibetan Plateau. *Sedimentary Geology* 454, 106462. <https://doi.org/10.1016/j.sedgeo.2023.106462>.
- Weltje, G.J., 2012. Quantitative models of sediment generation and provenance: state of the art and future developments. *Sedimentary Geology* 280, 4–20. <https://doi.org/10.1016/j.sedgeo.2012.03.010>.
- Weltje, G.J., von Eynatten, H., 2004. Quantitative provenance analysis of sediments: review and outlook. *Sedimentary Geology* 171 (1–4), 1–11. <https://doi.org/10.1016/j.sedgeo.2004.05.007>.
- Wu, L., Xiao, A., Wang, L., Shen, Z., Zhou, S., Chen, Y., Wang, L., Liu, D., Guan, J., 2011. Late Jurassic–Early Cretaceous Northern Qaidam Basin, NW China: implications for the earliest Cretaceous intracontinental tectonism. *Cretaceous Research* 32 (4), 552–564. <https://doi.org/10.1016/j.cretres.2011.04.002>.
- Wu, C., Yin, A., Zusa, A.V., Zhang, J., Liu, W., Ding, L., 2016. Pre-Cenozoic geologic history of the central and northern Tibetan Plateau and the role of Wilson cycles in constructing the Tethyan orogenic system. *Lithosphere* 8 (3), 254–292.
- Yan, Z., Yang, R., Yang, Y., Liu, Y., Galy, A., Fang, X., 2024. Late Miocene drainage reorganization on the NE Tibetan Plateau linked to growth of the Qilian Shan revealed by coupled carbonate Sr–silicate Nd isotopic tracers. *Palaeogeography, Palaeoclimatology, Palaeoecology* 638, 112038. <https://doi.org/10.1016/j.palaeo.2024.112038>.
- Yang, J., Wu, C., Zhang, J., Shi, R., Meng, F., Wooden, J., Yang, H.-Y., 2006. Protolith of eclogites in the north Qaidam and Altun UHP terrane, NW China: earlier oceanic crust? *Journal of Asian Earth Sciences* 28 (2–3), 185–204. <https://doi.org/10.1016/j.jseaes.2005.09.020>.
- Yang, S., Wang, Z., Guo, Y., Li, C., Cai, J., 2009. Heavy mineral compositions of the Changjiang (Yangtze River) sediments and their provenance-tracing implication. *Journal of Asian Earth Sciences* 35 (1), 56–65. <https://doi.org/10.1016/j.jseaes.2008.12.002>.
- Yang, S., Zhang, F., Wang, Z., 2012. Grain size distribution and age population of detrital zircons from the Changjiang (Yangtze) River system, China. *Chemical Geology* 296–297, 26–38. <https://doi.org/10.1016/j.chemgeo.2011.12.016>.
- Zhang, G., Song, S., Zhang, L., Niu, Y., 2008. The subducted oceanic crust within continental-type UHP metamorphic belt in the North Qaidam, NW China: evidence from petrology, geochemistry and geochronology. *Lithos* 104 (1–4), 99–118. <https://doi.org/10.1016/j.lithos.2007.12.001>.
- Zhang, S., Jian, X., Pullen, A., Fu, L., Liang, H., Hong, D., Zhang, W., 2020. Tectono-magmatic events of the Qilian orogenic belt in northern Tibet: new insights from detrital zircon geochronology of river sands. *International Geology Review* 63 (8), 917–940. <https://doi.org/10.1080/00206814.2020.1734876>.
- Zhuang, G., Hourigan, J.K., Ritts, B.D., Kent-Corson, M.L., 2011. Cenozoic multiple-phase tectonic evolution of the northern Tibetan Plateau: constraints from sedimentary records from Qaidam basin, Hexi Corridor, and Subei basin, northwest China. *American Journal of Science* 311 (2), 116–152. <https://doi.org/10.2475/02.2011.02>.
- Zoleikhaei, Y., Mulder, J.A., Cawood, P.A., 2021. Integrated detrital rutile and zircon provenance reveals multiple sources for Cambrian sandstones in North Gondwana. *Earth-Science Reviews* 213, 103462. <https://doi.org/10.1016/j.earscirev.2020.103462>.
- Zutterkirch, I.C., Kirkland, C.L., Barham, M., Elders, C., 2022. Thin-section detrital zircon geochronology mitigates bias in provenance investigations. *Journal of the Geological Society* 179 (2). <https://doi.org/10.1144/jgs2021-070>.